Accepted Manuscript

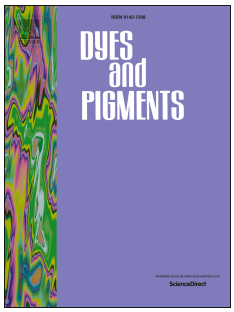

D-π-A benzo[*c*][1,2,5]selenadiazole-based derivatives *via* an ethynyl bridge: photophysical properties, solvatochromism and applications as fluorescent sensors

Hui Li, Yang Guo, Yunxiang Lei, Wenxia Gao, Miaochang Liu, Jiuxi Chen, Yuefei Hu, Xiaobo Huang, Huayue Wu

PII: S0143-7208(14)00277-0

DOI: 10.1016/j.dyepig.2014.06.035

Reference: DYPI 4443

To appear in: *Dyes and Pigments*

Received Date: 21 May 2014

Revised Date: 27 June 2014

Accepted Date: 29 June 2014

Please cite this article as: Li H, Guo Y, Lei Y, Gao W, Liu M, Chen J, Hu Y, Huang X, Wu H, D-π-A benzo[*c*][1,2,5]selenadiazole-based derivatives *via* an ethynyl bridge: photophysical properties, solvatochromism and applications as fluorescent sensors, *Dyes and Pigments* (2014), doi: 10.1016/j.dyepig.2014.06.035.

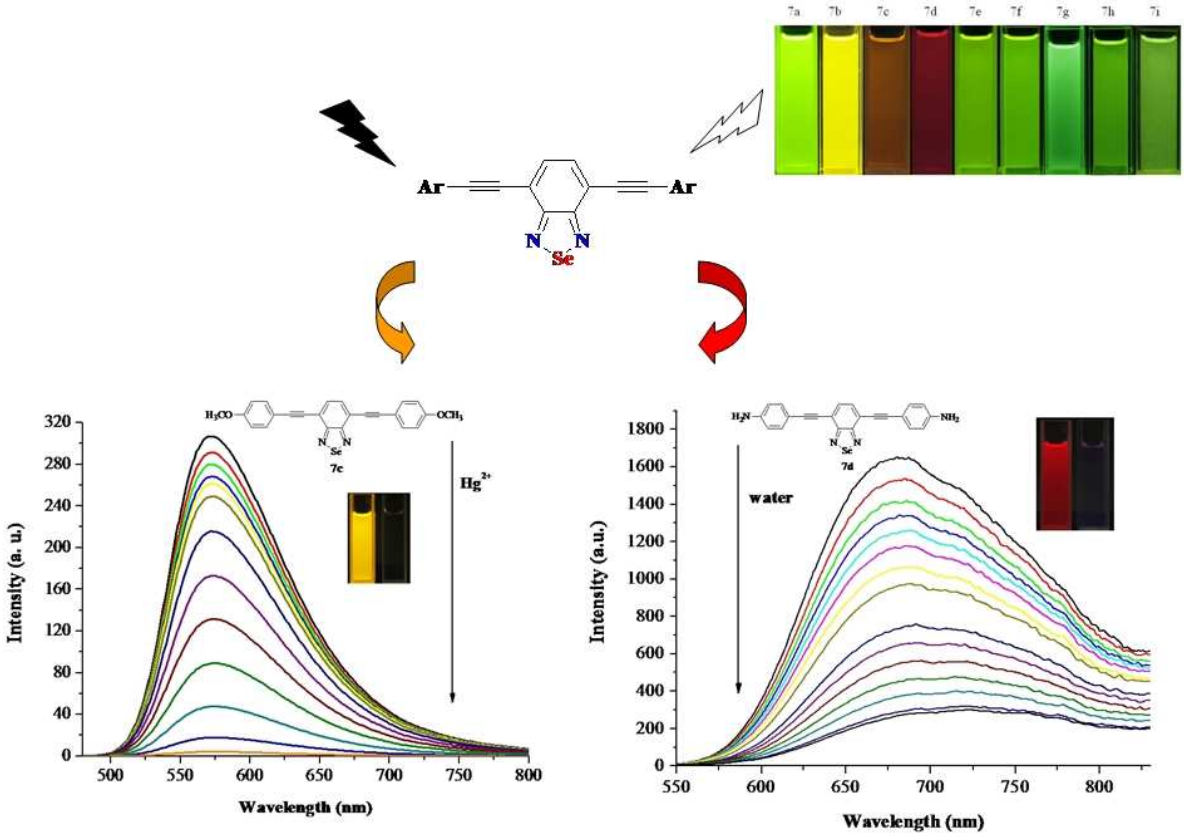

D-π-A benzo[*c*][1,2,5]selenadiazole-based derivatives *via* an ethynyl bridge: photophysical properties, solvatochromism and applications as fluorescent sensors

Hui Li[a], Yang Guo[b], Yunxiang Lei[a], Wenxia Gao[a], Miaochang Liu[a], Jiuxi Chen[a], Yuefei Hu[c], Xiaobo Huang[a,*], Huayue Wu[a,*]

[a]College of Chemistry and Materials Engineering, Wenzhou University, Wenzhou 325035, P. R. China

[b]School of Chemistry and Chemical Engineering, Nanjing University, Nanjing, 210093, P. R. China

[c]Department of Chemistry, Tsinghua University, Beijing 100084, P. R. China

*Corresponding authors. Tel.: +86 577 88368280; fax: +86 577 88368280

E-mail addresses: xiaobhuang@wzu.edu.cn (X. Huang); huayuewu@wzu.edu.cn (H. Wu)

ABSTRACT: A series of novel D-π-A benzo[*c*][1,2,5]selenadiazole (**BSe**)-based derivatives **7a-i** including electron-donating/electron-withdrawing groups were prepared by Pd-catalyzed Sonogashira- Hagihara reaction of 4,7-diethynylbenzoselenadiazole with various diiodo aryl compounds. Photophysical properties of these compounds were investigated by absorption and emission spectra analyses. Compound **7c** containing methoxy group exhibited positive solvatochromism and its solvatochromic properties were analyzed by the Lippert-Mataga equation and Kamlet-Taft equation, respectively. The resulting compounds showed tunable band gaps in the range of 2.21-2.70 eV using theoretical calculations, which was in good agreement with the results derived from the absorption of UV-vis spectra. In addition, fluorescent sensors **7c** and **7d** showed highly sensitive response for Hg^{2+} and traces of water using **BSe** as an acceptor or a fluorophore in real-time detection, respectively. These findings indicate that **BSe**-based molecules can be developed as excellent fluorophores for fluorescent material applications.

Keywords: Benzo[*c*][1,2,5]selenadiazole, photophysical properties, solvatochromism, fluorescent sensor

1. Introduction

Over the two decades, donor-π-acceptor (D-π-A) type organic fluorescent sensors have attracted much interest owing to their high sensitivity, selectivity and ease of measurement, and another fascinating advantage of such materials is that the π conjugation, band gap, and electro-optical properties can be effectively tuned by judicious choice of the fluorophores, donor and acceptor substituents. As a result, a lot of organic molecules have been developed as fluorophores in this kind of system for the fluorescent detection of ions [1], small organic molecules detection [2], and those structures with larger absorption and emission wavelengths also can be applied in biological and medical study [3]. Due to strong and stable fluorescence, good thermal stability and good electron-withdrawing ability, benzochalcogendiazoles, such as 2,1,3-benzothiadiazole (**BT**) plays

a very important position in the synthesis and application field of π-conjugated structure fluorescent sensors as an excellent fluorophore [4]. 2,1,3-Benzoselenadiazole (**BSe**) has a similar chemical structure as **BT**, but compared with **BT**, since the selenium atom has a much larger size and less electronegativity than the sulfur atom, it would have a more important influence for the heteroatoms on the optical properties of the **BSe**-based derivatives [5]. Recent years, comparison of effects caused by the heteroatom S and Se is becoming very common, it have been reported that **BSe**-based compounds showed obvious absorption and emission redshift than the **BT**-based compounds because **BSe** can more effectively lower the band gaps of these compounds and some of them exhibited interesting photoelectric properties [5a-e, 6].

To the best of our knowledge, there have few reports of the synthesis of D-π-A compounds containing **BSe** and aryl units join by an ethynyl bridge. The most possible reason is that dihalo compounds of **BSe** are hard to participate in the Sonogashira-Hagihara coupling reaction due to the poor reactivity and solubility influenced by the selenium atom. Recently, Bunz' group [7] and our group [8] successfully synthesized the key intermediate diethynylbenzoselenadiazole from **BT** by a strategy of firstly introducing the trimethylsilylacetylene flexible group, and then introducing the selenium atom. And then, this intermediate has been applied to the synthesis of a series of novel D-π-A polymers with low energy band gap incorporating a **BSe** moiety by us [8,9]. These polymers displayed obvious absorption peaks at the region from 477 to 510 nm, narrow orange-red or red fluorescence in the range of 576-595 nm, and their band gaps were in the range of 1.37-1.76 eV. Just as pointed out in the reported literatures [5a-e], these **BSe**-based polymers also showed outstanding absorption and emission redshift in comparison with the corresponding **BT**-based polymers. And one of them has been developed as a highly selective and sensitive chemosensor for heavy metal ions detection based on colorimetry and fluorometry [9]. In view of the very promising applications of these π-conjugated molecules based on **BSe**, their design, synthesis and photophysical properties are very attractive topics for researchers.

As a further extension of our research on the design of novel fluorophores for fluorescent materials [10], in this work, we described a series of D-π-A **BSe**-based derivatives **7a-j** by introducing appropriate electron donors and acceptors to **BSe** skeleton *via* an ethynyl linkage and systematically investigated their photophysical properties, solvatochromism, structure-property relationship and applications as fluorescent sensors. These compounds displayed obvious absorption peaks at the region from 429 to 488 nm and the fluorescence from green to red in the range of 512-669 nm in $CHCl_3$. Compound **7c** containing methoxy group exhibited positive solvatochromism and its solvatochromic properties were analyzed by the Lippert-Mataga equation and Kamlet-Taft equation, respectively. The HOMO-LUMO energy gaps of the resulting compounds derived from theoretical calculations has been compared with the results calculated by the photophysical measurements. In addition, fluorescent sensors **7c** and **7d** showed highly sensitive response for specific metal ion and traces of water using **BSe** as an acceptor or a fluorophore in real-time detection, respectively.

2. Experimental part

2.1. Materials

All solvents and reagents were commercially available and analytical-reagent-grade. THF and Et_3N were purified by distillation from sodium in the presence of benzophenone. 4,7-Dibromo-benzo[*c*][1,2,5]selenadioazole (**2**) and 3,6-dibromobenzene-1,2-diamine (**3**) could be prepared from **BT** (**1**) according to the literature reported by Myashi and coworkers [11], 3,6-bis(2-(trimethylsilyl)ethynyl)benzene-1,2-diamine (**4**), 4,7-bis(2-(trimethylsilyl)ethynyl)benzo[*c*][1,2,5]-selenadiazole (**5**) and 4,7-diethynylbenzoselenadiazole (**6**) could be prepared according to a reported procedure [8].

2.2. Measurements

Melting points were recorded on a Buchi Melting Point B-540 (uncorrected). The ^{1}H NMR and ^{13}C NMR spectra were recorded in solution of $CDCl_3$ or DMSO-d_6 on a Bruker DRX 500 NMR spectrometer with tetramethylsilane (TMS) as the internal standard. The chemical shift was recorded in ppm and the following abbreviations were used to explain the multiplicities: s = singlet, d = doublet, m = multiplet, br = broad. EI mass spectra were recorded on Agilent 5975C DIP/MS mass spectrometer. C, H and N of elemental analyses were performed on an Elementar Vario MICRO analyzer. UV-vis absorption was recorded on a Shimadzu UV-1700 spectrometer and fluorescence spectra were recorded on a RF-5301PC fluorometer. Thermogravimetric analysis (TGA) was performed on a Perkin-Elmer Pyris-1 instrument under a N_2 atmosphere.

*2.3. Preparation of **BSe**-based derivatives **7***

General procedure for synthesis of **BSe**-based derivatives **7**: A mixture of 4,7-diethynyl-benzoselenadiazole (**6**) (27.72 mg, 0.12 mmol), $Pd(PPh_3)_2Cl_2$ (4.21 mg, 0.006 mmol), CuI (2.30 mg, 0.012 mmol), PPh_3 (3.15 mg, 0.012 mmol) and diiodo aryl compound (0.36 mmol) was dissolved in 10 mL of Et_3N and 10 mL of THF. The reaction mixture was degassed and stirred at 60^{o}C for 12 h under a N_2 atmosphere. The solvent was removed under reduced pressure, and the residue was extracted with CH_2Cl_2. The organic layer was washed with water and then saturated sodium chloride solution, dried over anhydrous Na_2SO_4, and then evaporated in vacuum to dryness. The residue was purified by silica gel column chromatography with petroleum ether/chloroform (30:1, v/v) as an eluent to give the target compounds.

*4,7-Bis(2-phenylethynyl)benzo[c][1,2,5]selenadiazole (**7a**):* Yield: 60%; yellow solids; m. p. 141-142^{o}C; ^{1}H NMR ($CDCl_3$, 500 MHz): δ 7.71 (s, 2H), 7.68-7.66 (m, 4H), 7.41-7.38 (m, 6H); ^{13}C NMR ($CDCl_3$, 125 MHz): δ 159.3, 132.7, 132.0, 129.0, 128.4, 122.6, 119.0, 97.4, 85.7. FT-IR (KBr, cm^{-1}): 2921, 2848, 2359, 1653, 1490, 839. MS (EI): m/z: 383.9 [M^+]. Anal. Calcd for $C_{22}H_{12}N_2Se$: C, 68.94; H, 3.16; N, 7.31, found C, 69.05; H, 3.11; N, 7.24.

*4,7-Bis(2-p-tolylethynyl)benzo[c][1,2,5]selenadiazole (**7b**):* Yield: 65%; yellow solids; m. p. 256-257^{o}C; ^{1}H NMR (DMSO-d_6, 500 MHz): δ 7.79 (s, 2H), 7.52 (d, J = 7.5 Hz, 4H), 7.30 (d, J = 7.5 Hz, 4H), 2.37 (s, 6H); ^{13}C NMR (DMSO-d_6, 125 MHz): δ 158.3, 139.2, 132.2, 131.4, 129.5,119.1, 118.1, 96.6, 86.0. FT-IR (KBr, cm^{-1}): 2914, 2372, 1649, 1540, 1504, 839, 809. MS (EI): m/z: 411.9 [M^{+}]. Anal. Calcd for $C_{24}H_{16}N_2Se$: C, 70.07; H, 3.92; N, 6.81, found C, 69.89; H, 3.89; N, 6.85.

*4,7-Bis(2-(4-methoxyphenyl)ethynyl)benzo[c][1,2,5]selenadiazole (**7c**):* Yield: 75%; orange solids; m. p. 234-235^{o}C; ^{1}H NMR ($CDCl_3$, 500 MHz): δ 7.66 (s, 2H), 7.60 (d, J = 8.5 Hz, 4H), 6.92 (d, J = 9.0 Hz, 4H), 3.85 (s, 6H); ^{13}C NMR ($CDCl_3$, 125 MHz): δ 160.2, 159.4, 133.6, 132.4, 118.9, 114.8, 114.1, 97.6, 84.9, 55.4. FT-IR (KBr, cm^{-1}): 2921, 2848, 2354, 1600, 1507, 826. MS (EI): m/z: 443.9 [M^{+}]. Anal. Calcd for $C_{24}H_{16}N_2O_2Se$: C, 65.02; H, 3.64; N, 6.32, found C, 64.97; H, 3.61; N, 6.39.

*4,7-Bis(2-(4-aminophenyl)ethynyl)benzo[c][1,2,5]selenadiazole (**7d**):* Yield: 62%; red solids; m. p. 250-251^{o}C; ^{1}H NMR ($CDCl_3$, 500 MHz): δ 7.56 (s, 2H), 7.39 (d, J = 7.0 Hz, 4H), 6.61 (d, J = 6.5 Hz, 4H); ^{13}C NMR ($CDCl_3$, 125 MHz): δ 159.3, 147.5, 133.3, 131.8, 118.6, 114.5, 111.4, 98.4, 84.2. FT-IR (KBr, cm^{-1}): 3431, 2915, 2842, 2346, 1597, 1507, 833. MS (EI): m/z: 413.9 [M^{+}]. Anal. Calcd for $C_{22}H_{14}N_4Se$: C, 63.93; H, 3.41; N, 13.55, found C, 64.02; H, 3.38; N, 13.60.

*4,7-Bis(2-(4-fluorophenyl)ethynyl)benzo[c][1,2,5]selenadiazole (**7e**):* Yield: 70%; yellow solids; m. p. 267-268^{o}C; ^{1}H NMR ($CDCl_3$, 500 MHz): δ 7.70 (s, 2H), 7.66-7.64 (m, 4H), 7.11-7.08 (m, 4H); ^{13}C NMR ($CDCl_3$, 125 MHz): δ 163.0 (d, J = 249.4 Hz), 159.2, 133.9, 132.6, 118.8 (d, J = 25.3 Hz), 115.8 (d, J = 22.1 Hz), 114.1, 96.3, 85.5. FT-IR (KBr, cm^{-1}): 2924, 2848, 2359, 1507, 835. MS (EI): m/z: 419.9 [M^{+}]. Anal. Calcd for $C_{22}H_{10}F_2N_2Se$: C, 63.02; H, 2.40; N, 6.68, found C, 62.90; H, 2.46; N, 6.79.

*4,7-Bis(2-(4-chlorophenyl)ethynyl)benzo[c][1,2,5]selenadiazole (**7f**):* Yield: 66%; yellow solids; m. p. 251-252^{o}C; ^{1}H NMR ($CDCl_3$, 500 MHz): δ 7.71 (s, 2H), 7.59 (d, J = 8.5 Hz, 4H), 7.37 (d, J = 8.0 Hz, 4H); ^{13}C NMR ($CDCl_3$, 125 MHz): δ 159.1, 135.1, 133.2, 130.9, 128.8, 125.0, 118.9, 96.4, 86.8. FT-IR (KBr, cm^{-1}): 2915, 2849, 2352, 1649, 1490, 824. MS (EI): m/z: 451.8 [M^{+}]. Anal. Calcd for $C_{22}H_{10}Cl_2N_2Se$: C, 58.43; H, 2.23; N, 6.19, found C, 58.51; H, 2.19; N, 6.05.

*4,7-Bis(2-(4-nitrophenyl)ethynyl)benzo[c][1,2,5]selenadiazole (**7g**):* Yield: 65%; yellow solids; m. p. 210-211^{o}C; ^{1}H NMR ($CDCl_3$, 500 MHz): δ 8.28 (d, J = 8.5 Hz, 4H), 7.82 (d, J = 8.5 Hz, 4H), 7.79 (s, 2H); ^{13}C NMR ($CDCl_3$, 125 MHz): δ 159.0, 147.5, 133.2, 132.7, 129.2, 123.7, 118.9, 95.5, 90.2. FT-IR (KBr, cm^{-1}): 2914, 2848, 2365, 1590, 1507, 859. MS (EI): m/z: 473.8 [M^{+}]. Elemental Anal. Calcd for $C_{22}H_{10}N_4O_4Se$: C, 55.83; H, 2.13; N, 11.84, found C, 55.90; H, 2.06; N, 11.78.

*4,7-Bis(2-(4-(trifluoromethyl)phenyl)ethynyl)benzo[c][1,2,5]selenadiazole (**7h**):* Yield: 60%; yellow solids; m. p. 253-254^{o}C; ^{1}H NMR ($CDCl_3$, 500 MHz): δ 7.77 (d, J = 8.0 Hz, 4H), 7.75 (s, 2H), 7.66 (d, J = 8.0 Hz, 4H); ^{13}C NMR ($CDCl_3$, 125 MHz): δ 159.1, 133.0, 132.2, 130.7 (d, J = 32.6 Hz), 126.2, 125.4, 123.8 (d, J = 270.6 Hz), 118.9, 95.9, 87.6. FT-IR (KBr, cm^{-1}): 2928, 2855, 2358, 1613, 1504, 841. MS (EI): m/z: 519.9 [M^+]. Anal. Calcd for $C_{24}H_{10}F_6N_2Se$: C, 55.51; H, 1.94; N, 5.39, found C, 55.42; H, 1.89; N, 5.46.

*4,7-Bis(2-(pyridin-2-yl)ethynyl)benzo[c][1,2,5]selenadiazole (**7i**):* Yield: 62%; yellow solids; m. p. 207-208^{o}C; ^{1}H NMR ($CDCl_3$, 300 MHz): δ 8.69-8.68 (m, 2H), 7.79 (s, 2H), 7.74-7.67 (m, 4H), 7.31-7.26 (m, 2H); ^{13}C NMR ($CDCl_3$, 125 MHz): δ 159.1, 150.3, 142.9, 136.2, 133.3, 127.6, 123.3, 118.8, 96.4, 85.1. FT-IR (KBr, cm^{-1}): 2921, 2848, 2359, 1646, 1576, 1454, 844, 832. MS (EI): m/z: 385.9 [M^+]. Anal. Calcd for $C_{20}H_{10}N_4Se$: C, 62.35; H, 2.62; N, 14.54, found C, 62.47; H, 2.70; N, 14.42.

*2.4. Metal ion titration of **7c** and the detection for traces of water of **7d***

Each metal ion titration experiment was started with a 3.0 mL **7c** in THF solution with a known concentration (1.0×10^{-5} mol·L^{-1}). Mercury perchlorate salt and other various metal salts (nitrate, 1.0×10^{-3} mol·L^{-1}, CH_3CN) were used for the titration. The concentration of **7d** was fixed at 1.0×10^{-5} mol·L^{-1} in anhydrous THF and the aqueous THF (water:THF = 1:9, v/v) for titration was deionized water. Because the minimum response time that can be measured is limited in the manipulation time, all kinds of measurements were monitored 10 s after the addition of the metal salt or water to the host molecule solutions for the application of real-time detection.

3. Results and discussion

*3.1 Synthesis of **BSe**-based derivatives*

Scheme 1 illustrated the synthetic routes to target **BSe**-based derivatives **7a-i**. The key intermediate 4,7-diethynylbenzo[*c*][1,2,5]selenadiazole (**6**) was designed to be synthesized by a strategy of firstly introducing the trimethylsilylacetylene flexible group, and then introducing the selenium atom from the starting material **BT** (**1**). And then **BSe** derivatives **7a-i** was synthesized by Pd-catalyzed Sonogashira-Hagihara reaction from compound **6** with various commercially available diiodo aryl compounds in 60-75% yields. These target compounds were fully characterized by ^{1}H NMR, ^{13}C NMR, EI mass spectra and elemental analysis, etc. Thermal stability is one of the key requirements for practical applications of organic fluorophores. The thermal properties of **7a-i** were investigated by TGA, which were carried out under a N_2 atmosphere at a heating rate of 10°C/min. As shown in Fig. 1, although these compounds have a similar structure, their TGA plots are different. The TGA curves reveal that the degradation temperature (T_d) of 5% weight loss of **7a-i** was in the range of 211-378°C. There is a total loss of

about 32-50% for **7a-i** when heated to 700°C, respectively. The results indicate these **BSe** derivatives can provide a desirable thermal property for various fluorescent materials.

*3.2 Optical properties of compounds **7a-i***

The resulting compounds **7a-i** are soluble in common organic solvents such as $CHCl_3$, dichloromethane (DCM), THF, Acetone, DMSO, dimethylformamide (DMF), CH_3CN and toluene, etc. Their UV-vis absorption and emission spectra were measured in $CHCl_3$ as shown in Fig. 2 and Fig. 3, respectively, and the data are presented in Table 1. These compounds have well-resolved absorption peaks in the range of 235 to 500 nm, and the band situated at a short wavelength 300-350 nm region is assigned to the localized π-π* transition [12]. And in view of maximum absorption wavelengths (λ_{abs}^{max}) of these compounds, all of them have strong absorption at a long wavelength 420-500 nm region compared to compound **6** (393 nm) due to its coplanarity of **BSe** unit and aryl group *via* triple bond as well as the charge transfer from aryl group to **BSe** unit [13].

The fluorescence quantum yields (Φ_F) of **7a-i** were determined in $CHCl_3$ at room temperature using the quinine sulfate solution as a fluorescence reference (Φ_r = 0.55 in 0.5 mol/L H_2SO_4). The Φ_F values could be calculated using the equation [14]: $\Phi_F = \Phi_r (F_s/F_r)(A_r/A_s)(\eta_s/\eta_r)^2$, where s and r denote the sample and reference, respectively, F is the integrated fluorescence intensity, A is the absorbance at the excited wavelength, and η is the refractive index of the solvent. As shown in Table 1, it can be found that all these compounds have high quantum yields (Φ_F = 0.17-0.37) owing to D-π-A structure, with the exception of **7d** (Φ_F = 0.04) containing a NH_2 group which quenches fluorescence. As shown in Fig. 3 and Fig. 4, it can be found that these compounds show tunable emission wavelengths by introducing appropriate electron donors and acceptors to **BSe** skeleton *via* an ethynyl linkage, and emit such as green, yellow, orange and red fluorescence under a 365 nm UV lamp, respectively. The maximum fluorescence emission wavelengths (λ_{em}^{max}) of compounds **7b-d** including electron-donating groups have obvious redshift relative to **7a** (546 nm) containing only phenyl group. And among these compounds, the strongest donor substituted **7d** appears emission peak situated at 669 nm, and has as high as 123 nm red shift and shows red fluorescence, whereas, compounds **7g-i** containing strong electron-withdrawing groups show obvious blue shift (19-33 nm). All these compounds show large Stokes shifts (77-181 nm) which is beneficial for the detection of emission wavelength by avoiding the interference from the excitation wavelength, especially for **7c** and **7d**, the large Stokes shifts indicate a very efficient intramolecular charge transfer (ICT) in the excited state between the terminal methoxy group or NH_2 group and the **BSe** unit [3h]. Compared with those corresponding **BT**-based compounds which have the some structure with **7a** and **7c** [15], **7a** and **7c** exhibit about 20-60 nm redshift in absorption and emission spectra. These results indicate that the π-conjugated organic compounds are good candidates for wavelength-shifting material development.

*3.3 Fluorescence change of compounds **7a-i** toward solve polarity*

D-π-A organic compounds often show solvatochromism which is based on the interaction between the solvent molecules and a fluorophore, and solvent-dependent changes in the spectra of these solvatochromic compounds provide a sensitive response to changes in the surrounding environment [16]. Based on the polarity of organic solvent varied, the solvatochromic changes of these compounds were studied. Herein, we firstly studied the solvatochromism of **7c**. The UV-vis and fluorescence spectra of **7c** in various solvents, such as toluene, $CHCl_3$, THF, DCM, DMF, acetone and CH_3CN, are shown in Fig. 5 and Fig. 6, and the absorption and emission data have been listed in Table 2, respectively. The results indicate that compound **7c** containing strong electron-donating methoxy group presents similar absorption spectra in different polar solvents, whereas, displays obvious red shift changes of fluorescence spectra from 553 nm to 604 nm as increasing solvent polarity from toluene to CH_3CN. Visible fluorescence of **7c** in various solvents appears visual color change from green to red, which can be clearly observed under a 365 UV lamp (Fig. 7). The results indicate **7c** shows solvent polarity dependence.

There are several independent modes of fluorophore-solvent interaction identified for solvatochromism, and one of the most used quantitative treatments of the solvent effects is the $E_T(30)$ scale introduced by Reichardt [17]. $E_T(30)$ values were derived from the long-wavelength vis/near-IR absorption band of a negatively solvatochromic pyridinium N-phenolate betaine dye. The dependence of the emission maxima of **7c** on $E_T(30)$ solvent polarity parameter [18] can be fitted to linear function and the correlation coefficients R = 0.89 (Fig. 8). As the solvent polarity increased, a positive solvatochromic shift can be observed.

The influence of solvent polarity on the optical properties of a fluorophore can be studied by Lippert-Mataga equation: $\Delta\nu = \nu_{abs}-\nu_{em} = 2(\mu_e-\mu_g)^2\Delta f/hca^3+C$, a model that describes the interactions between the solvent and the dipole moment of a fluorophore [19]. In the equation, μ_e and μ_g are the dipole moments in the excited and ground states, respectively, h is the Planck constant, c is the speed of light, a is the radius of the fluorophore and $\Delta\nu$ is Stokes shifts of fluorescence spectra. Δf is called the orientation polarizability, which can be expressed as $(\varepsilon-1)/(2\varepsilon+1)-(n^2-1)/(2n^2+1)$, herein, ε and n are the dielectric constant and refractive index of solvent, respectively. Δf values for the various solvents could be calculated from known values of ε and n (Table 2). The Lippert-Mataga plot of **7c** is depicted in Fig. 9. It can be found that the plot of $\Delta\nu$ against Δf in these different polar solvents has a positive correlation and is nearly linear with correlation coefficient R = 0.92. The positive linear dependence suggests that the excited-state of **7c** has a larger dipole moment than the ground-state. The obvious solvatochromic redshift of **7c** can be attributed to ICT effect on the fluorescent emission, which leads to the decrease of the energy level and solvent stabilization of excited state. This effect becomes larger as the solvent polarity increases, resulting in the emission at a longer wavelength [20]. As a result, emissions of **7c** depend on the solvent polarity and the fluorescence color changes can be directly detected by naked eyes under UV-lamp. We further studied the plots of $\Delta\nu$ of the other compounds *vs* Δf. The UV-vis and fluorescence spectra of the other compounds in various solvents are shown in Fig. S1

and Fig. S2 (See Supporting Information), and the absorption and emission data are listed in Table S1 and Table S2 (See Supporting Information), respectively. The results indicate that the optical properties of all of these compounds also show different degrees of positive solvent dependence (Fig. S3, see Supporting Information), and in these compounds, **7d** exhibits the steepest slope, indicating the largest fluorescence solvatochromism which could be due to the strongest electron donating ability of NH_2 group. Thus, we can construct colorful fluorophores based on **BSe** derivatives which can form an ICT state that is normally sensitive to the solvent polarity, which also implies these kinds of compounds might be applied to the development of efficient sensors for the detection of volatile organic compounds (VOCs).

Considering not only the polarity but also the acidity and the basicity of the solvents, the solvatochromic Stokes shifts and emission bands of **7c** can be calculated based on Kamlet-Taft equation [21]: $Y = Y_0+a\alpha+b\beta+c\pi^*$. Herein, Y_0 is the property of substance in the absence of solvent e.g. in the gas-phase, α, β and π^* are the solvent parameters that characterize the acidity, the basicity and polarity of the solvent, respectively. a, b and c are the corresponding coefficients. The corresponding α, β and π^* values of various solvents used in this study for calculating the emission wavenumbers at the maximum (ν_{em}) and the Stokes shifts ($\Delta\nu$) are given in Table S3 (See Supporting Information). The Kamlet-Taft coefficients for ν_{em} and $\Delta\nu$ can be obtained by multilinear regression analysis. According to the regression analysis for ν_{em} and $\Delta\nu$, the relationships can be established as follows:

ν_{em} (cm^{-1}) = (19271±168)-(4181±436)α-(1173±167)β-(2150±289)π^*

$\Delta\nu$ (cm^{-1}) = (2642±404)+(5074±1052)α+(2087±404)β+(1508±697)π^*

For the sake of better visualization of the experimental and the fitted data, the calculated values of ν_{em} and $\Delta\nu$ are listed in Table 2 and plotted against measured values in Fig. 10, respectively. As shown in Fig. 10, it can be found that the measured values for ν_{em} and $\Delta\nu$ are correlated well with those of the calculated by Kamlet-Taft equation, and the correlation coefficients R = 0.99 and 0.98, respectively. As a result of these calculations, it is now evident that the Kamlet-Taft theory is capable of describing the solvatochromic behavior of **7c** in a wide variety of solvents.

3.6. Molecular orbital calculations

We performed density functional theoretical (DFT) calculations to gain a better understanding of the geometric, electronic structure and optical properties of the molecules presented in the study. All calculations were carried out with the Gaussian 03, Revision C. 02 program [22], using the Becke's three-parameter set with Lee-Yang-Parr modification (B3LYP) with 6-31+G** basis set. Fig. 11 displays the LUMO and the HOMO diagrams of compounds **7a-i** and the calculated HOMO, LUMO and E_g are listed in Table 1.

According to Fig. 11, the LUMO distributions of these compounds mainly reside on the central **BSe** core, and the HOMO distributions are predominantly located on the **BSe** core and substituted phenyl rings. Thus, the excited states of these compounds can be assigned to π-π* transition mixed

with ICT process in this system. This is in accordance with the experimental results of the dependence on the solvent polarity for the fluorescence spectra of these compounds. As seen from Table 1, it can be found that the HOMO energy levels of **7b-d** containing electron donor group are higher than **7e-i** containing electron acceptor group because of the electron-donating ability of the donor unit, such as **7d** and **7g** show the highest HOMO energy (-4.86 eV) and the lowest HOMO energy (-6.18 eV), respectively. It also can be found **7e-i** have lower HUMO energy levels compared to **7b-d** because strong electron acceptor group can effectively reduce the energy of LUMO, and in these compounds, **7g** has lowest LUMO energy (-3.60 eV). The band gaps (E_g) of **7a-i** are in the range of 2.21 eV and 2.70 eV, and **7d** has the lowest band gap (2.21 eV) which can be mainly attributed that NH_2 group with strongest electron-donating ability greatly increases the HOMO energy of the compound. The energy gaps obtained from the theoretical calculations and UV-vis absorption maxima are described in Fig. 12. Apart from a slight variation for each compound, there is a satisfactory correlation of the data from the theoretical calculations and UV-vis absorption maxima in that all compounds show a similar trend except **7i**.

*3.4. The fluorescence response of **7c** on Hg^{2+}*

BT unit has been reported as a good receptor for the recognition of specific metal ion, such as Hg^{2+} and Ni^{2+} in some previous reports [4]. In comparison with **BT**, **BSe** used as recognition moiety might weaken the binding capacity to other metal ions except a specific metal ion, and then improve the selectivity of the **BSe**-based fluorescent sensor. Herein, we studied the ability of compound **7c** to identify metal ions using **BSe** as recognition site. Compound **7c** displayed orange fluorescence centered at 575 nm when excited at λ_{ex} = 458 nm in THF. In order to provide a potential ‘‘zero-wait’’ detecting method for metal ions, we investigated the fluorescence response behaviors of **7c** upon the addition of various metal ions in real-time detection, all kinds of measurements were monitored 10 s after addition of the metal salt to the host molecule solutions. Fig. 13 shows the fluorescence spectra of **7c** in THF solution (1.0×10^{-5} mol·L^{-1}) with Hg^{2+} in CH_3CN concentrations from 0 to 4.5×10^{-5} mol·L^{-1}. As is evident from Fig. 13, upon the addition of Hg^{2+}, obvious fluorescence quenching can be observed. Hg^{2+} led to about 94% quenching of **7c** fluorescence at a concentration of 4.0×10^{-5} mol·L^{-1}. In addition, the orange color of the compound fluorescence disappeared after the addition of Hg^{2+}, which could be easily detected by naked eyes (Fig. 13, inset). The quenching effect could be attributed to the intramolecular photoinduced charge transfer between **7c** and the **BSe**-Hg^{2+} complex. Notably, there exists a good linear relationship between the changes in fluorescence intensity of **7c** and the Hg^{2+} concentration, a curve equation is got in the range of Hg^{2+} concentrations from 0 to 4.0×10^{-5} mol·L^{-1} is $F = 3.43\times10^{4}\text{-}7.85\times10^{8}$ [Hg^{2+}], R = 0.997, N = 13, which indicates that Hg^{2+} can be quantitative detection (Fig. 14). According to the equation and the standard deviation of the blank, the fluorescence detection limit of **7c** for Hg^{2+} was determined to be 5.0×10^{-7} mol·L^{-1}. The quenching efficiency of a sensor can be described by the Stern-Volmer equation: $F_0/F = 1 + K_{SV}[Q]$, herein,

F_0 and F are the fluorescence intensities in the absence and presence of a quencher, respectively, K_{SV} is the quenching constant and [Q] is the quencher concentration. At low concentrations of Hg^{2+} (0 to 1.0×10^{-5} mol·L^{-1}), a linear Stern-Volmer plot was obtained with the K_{SV} value of 2.46×10^{5} mol^{-1}·L, however, at high concentrations, the plot was found to be non-linear, showing positive curvature as show in Fig. 15. The nonlinearity suggests the mechanism of the quenching process may involve a combination of complexation and collisional processes [23].

To test the selectivity of the sensor for Hg^{2+}, the fluorescence response behaviors of **7c** on other important metal ions at a concentration of 2.0×10^{-4} mol·L^{-1} were performed (Fig. 16). All these metals induced little fluorescence change, the degree of fluorescence quenching ($1-F/F_0$) of **7c** were no more than 6% by other metal ions, such as K^+, Pb^{2+}, Cu^{2+}, Co^{2+}, Cd^{2+}, Fe^{3+}, Mn^{2+}, Ni^{2+}, Zn^{2+} and Ag^+ at a high mole ratio of 4:1, which could be attributed to the poor coordination ability of the compound with these metal ions and the unmatched radius of the metal ions. The results indicate **7c** exhibits excellent selectivity for Hg^{2+} sensing. For effective Hg^{2+} detection, another essential requirement is no or less interference from other metal ions. The Hg^{2+} detection experiments of the **7c** solution were performed in the presence of 4.0×10^{-5} mol·L^{-1} of other metal ions (Fig. 17). The deviation of the fluorescence quenching in the presence of other metals ions was less than 5%. The results demonstrated the Hg^{2+} detection showed no significant interference from other metal ions. The high sensitivity and selectivity toward Hg^{2+} of the compound may be attributed to several factors, such as the structural rigidity of the **BSe** unit, the larger radius of the Hg^{2+} ion and preferred coordination arrangement of Hg^{2+}, soft acid/base characteristics of **BSe** and Hg^{2+} [24]. These results indicate that **BSe** unit could function as recognition moiety for Hg^{2+} probe with high selectivity and sensitivity.

*3.5. The fluorescence response of **7d** on water*

BSe unit also can be used as a fluorophore of D-π-A **BSe**-based fluorescent sensors for detecting the other species by introducing some specific recognition sites on the parent structure. Brown and Yuan reported that the fluorescent quantum yield and lifetime of 4-aminonaphthalimide both decreased with the increased water content of the system, which can be attributed to the formation of a hydrogen-bonded cluster between the probe and the water molecules by NH_2 group [25]. This fact indicates that **7d** might be used as an efficient water sensor, using amino group as an acceptor and **BSe** unit as a fluorophore. Herein, we investigated the effects of the fluorescence response behaviors of **7d** on water in real-time detection. Fig. 18 and Fig. 19 show the fluorescence spectra and intensity of **7d** (1.0×10^{-5} mol·L^{-1} in anhydrous THF) upon the water content from 0 to 1.83% in THF, respectively. It could be found that the spectra exhibited significant fluorescence quenching with an obvious redshift in the emission maxima as the water content increased. When the water content was increased to be 1.83% (v/v), the degree of fluorescence quenching was 81%, and the red color of **7d** fluorescence disappeared (Fig. 18, inset). When **7d** was used to determine the water content, the changes of fluorescence intensity fit

well with a Stern-Volmer equation as a function of the water content: F_0/F = 1 + 2.38 [H_2O], herein, [H_2O] was the percentage of the volume of water and THF, and K_{SV} was 2.38 (Fig. 20). The results indicate that compound **7d** containing amino group can be developed to be a good fluorescent sensor for the quantitative detection of traces of water in organic solvent.

4. Conclusion

A series of novel D-π-A **BSe**-based derivatives **7a-i** with tuneable absorption and emission wavelengths over a wide range by introducing strong electron-donating/electron-withdrawing groups into a **BSe** unit were designed and synthesized. These compounds showed obvious absorption peaks at the region from 429 to 488 nm, the fluorescence from green to red in the range of 512-669 nm and high quantum yields. The HOMO-LUMO energy gaps of **7a-i** obtained using theoretical calculations were in the range of 2.21-2.70 eV, which were in good agreement with those derived from the absorption of UV-vis spectra. Compound **7c** containing methoxy group exhibited positive solvatochromism, which indicates these kinds of arylethynylene materials containing **BSe** might be used for solvent polarity sensors. In addition, fluorescent sensors **7c** and **7d** showed highly sensitive response for mercury ion and traces of water using **BSe** as an acceptor or a fluorophore in real-time detection, respectively. These findings indicate that **BSe**-based molecules can be developed as excellent fluorophores for fluorescent material applications.

Acknowledgements

This work was supported by the National Natural Science Foundation of China (No. 21204066), Commonweal Project of Science and Technology Department of Zhejiang Province (No. 2012C23030, 2013C33188) and the Bureau of Science and Technology of Wenzhou (No. S20100007).

References

[1] (a) de Silva AP, Gunaratne HQN, Gunnlaugsson T, Huxley AJM, McCoy CP, Rademacher JT, Rice TE. Signaling recognition events with fluorescent sensors and switches. Chem Rev 1997;97:1515-66;

(b) Zucchero AJP, McGrier, L, Bunz UHF. Cross-conjugated cruciform fluorophores. Acc Chem Res 2010;43:397-408;

(c) Guo Z, Zhu W, Tian H. Dicyanomethylene-*4H*-pyran chromophores for OLED emitters, logic gates and optical chemosensors. Chem Commun 2012;48:6073-84;

(d) Achelle S, Baudequin C, Plé N. Luminescent materials incorporating pyrazine or quinoxaline moieties. Dyes Pigm 2013;98:575-600;

(e) Wagner S, Brödner K, B. Coombs A, Bunz UHF. Pyridine-substituted BODIPY as fluorescent probe for Hg^{2+}. Eur J Org Chem 2012:2237-42;

(f) Guo Z, Zhu W, Tian H. Hydrophilic copolymer bearing dicyanomethylene-*4H*-pyran moiety as

fluorescent film sensor for Cu^{2+} and pyrophosphate anion. Macromolecules 2010;43:739-44;

(g) Nguyen DM, Frazer A, Rodriguez L, Belfield KD. Selective fluorescence sensing of zinc and mercury ions with hydrophilic 1,2,3-triazolyl fluorene probes. Chem Mater 2010;22:3472-81;

(h) Ye C, Sun B, Wang X, Yang J, Ding P, Zhu S, He Q, Liang Z, Tao X. Synthesis and two-photon up-conversion sensing property of pyridinylbenzothiadiazole-based chromophores. Dyes Pigm 2014;102:133-41;

(i) Zheng SL, Lin N, Reid S, Wang B. Effect of extended conjugation with a phenylethynyl group on the fluorescence properties of water-soluble arylboronic acids. Tetrahedron 2007;63:5427-36;

(j) Liu S, Shi Z, Xu W, Yang H, Xi N, Liu X, Zhao Q, Huang W. A class of wavelength-tunable near-infrared aza-BODIPY dyes and their application for sensing mercury ion. Dyes Pigm 2014;103:145-53;

(k) Xiang G, Cui W, Lin S, Wang L, Meier H, Li L, Cao D. A conjugated polymer with ethyl 2-(2-(pyridin-2-yl)-*1H*-benzo[*d*]imidazol-1-yl)acetate units as a novel fluorescent chemosensor for silver(I) detection. Sensor Actuat B Chem 2013;186:741-9.

[2] (a) Zhang X, Ren X, Xu QH, Loh KP, Chen ZK. One- and two-Photon turn-on fluorescent probe for cysteine and homocysteine with large Emission Shift. Org Lett 2009;11:1257-60;

(b) Ji S, Yang J, Yang Q, Liu S, Chen M, Zhao J. Tuning the intramolecular charge transfer of alkynylpyrenes: effect on photophysical properties and its application in design of OFF-ON fluorescent thiol probes. J Org Chem 2009;74:4855-65;

(c) Zhang X, Chi L, Ji S, Wu Y, Song P, Han K, Guo H, James TD, Zhao J. Rational design of d-PeT phenylethynylated-carbazole monoboronic acid fluorescent sensors for the selective detection of α-hydroxyl carboxylic acids and monosaccharides. J Am Chem Soc 2009;131:17452-63;

(d) Long Y, Chen H, Wang H, Peng Z, Yang Y, Zhang G, Li N, Liu F, Pei J. Highly sensitive detection of nitroaromatic explosives using an electrospun nanofibrous sensor based on a novel fluorescent conjugated polymer. Anal Chim Acta 2012;744:82-91.

[3] (a) Carroll CN, Naleway JJ, Haley MM, Johnson DW. Arylethynyl receptors for neutral molecules and anions: emerging applications in cellular imaging. Chem Soc Rev 2010;39:3875-88;

(b) Aranda AI, Achelle S, Hammerer F, Mahuteau-Betzer F, Teulade-Fichou MP. Vinyl-diazine triphenylamines and their *N*-methylated derivatives: synthesis, photophysical properties and application for staining DNA. Dyes Pigm 2012;95:400-7;

(c) Lin HH, Chan YC, Chen JW, Chang CC. Aggregation-induced emission enhancement characteristics of naphthalimide derivatives and their applications in cell imaging. J Mater Chem 2011;21:3170-7;

(d) Cheng T, Xu Y, Zhang S, Zhu W, Qian X, Duan L. A highly sensitive and selective OFF-ON fluorescent sensor for cadmium in aqueous solution and living cell. J Am Chem Soc 2008;130:16160-1;

(e) Vedamalai M, Wu SP. A BODIPY-based colorimetric and fluorometric chemosensor for Hg(II) ions and its application to living cell imaging. Org Biomol Chem 2012;10:5410-6;

(f) Zheng Z, Zhang Q, Yu Z, Yang M, Zhou H, Wu J, Tian Y. Four new two-photon absorbing imidazo[4,5-*f*]1,10-phenanthroline dye derivatives with different dipole moment orientation based on different groups: synthesis, optical characterization and bioimaging. J Mater Chem C 2013;1:822-30;

(g) Liu XD, Xu Y, Sun R, Xu YJ, Lu JM, Ge JF. A coumarin-indole-based near-infrared ratiometric pH probe for intracellular fluorescence imaging. Analyst 2013;138:6542-50;

(h) Neto BAD, Lapis AAM, Mancilha FS, Vasconcelos IB, Thum C, Basso LA, Santos DS, Dupont J. New sensitive fluorophores for selective DNA detection. Org Lett 2007;9:4001-4.

[4] (a) Liu SJ, Fang C, Zhao Q, Fan QL, Huang W. A highly selective, colorimetric, and fluorometric multisignaling chemosensor for Hg^{2+} based on poly(*p*-phenyleneethynylene) containing benzo[2,1,3]thiadiazole. Macromol Rapid Commun 2008;29:1212-15;

(b) Huang XB, Meng J, Dong Y, Cheng YX, Zhu CJ. Polymer-based fluorescence sensors incorporating chiral binaphthyl and benzo[2,1,3]thiadiazole moieties for Hg^{2+} detection. J Polym Sci Part A Polym Chem 2010;48:997-1006;

(c) Huang XB, Xu Y, Zheng LF, Meng J, Cheng YX. A highly selective and sensitive fluorescence chemosensor based on optically active polybinaphthyls for Hg^{2+}. Polymer 2009;50:5996-6000;

(d) Huang XB, Dong Y, Meng J, Cheng YX, Zhu CJ. The fluorescence polymer incorporating triazole and benzo[2,1,3]thiadiazole moieties for Ni^{2+} detection. Synlett 2012;12:1841-4;

(e) Li J, Meng J, Huang XB, Cheng YX, Zhu CJ. A highly selective fluorescent sensor for Hg^{2+} based on the water-soluble poly(*p*-phenyleneethynylene). Polymer 2010;51:3425-30;

(f) Ma X, Song FY, Wang L, Cheng YX, Zhu CJ. Polymer-based colorimetric and “turn off” fluorescence sensor incorporating benzo[2,1,3]thiadiazole moiety for Hg^{2+} detection. J Polym Sci Part A Polym Chem 2012;50:517-22.

[5] (a) Yang R, Tian R, Yang W, Hou Q, Cao Y. Synthesis and optical and electroluminescent properties of novel conjugated copolymers derived from fluorene and benzoselenadiazole. Macromolecules 2003;36:7453-60;

(b) Yang R, Tian R, Yan J, Zhang Y, Yang J, Hou Q, Yang W, Zhang C, Cao Y. Deep-red electroluminescent polymers: synthesis and characterization of new low-band-gap conjugated copolymers for light-emitting diodes and photovoltaic devices. Macromolecules 2005;38:244-53;

(c) Hou J, Chen TL, Zhang S, Chen HY, Yang Y. Poly[4,4-bis(2-ethylhexyl)cyclopenta-[2,1-b;3,4-b#]dithiophene-2,6-diyl-*alt*-2,1,3-benzoselenadiazole-4,7-diyl], a new low band gap polymer in polymer solar cells. J Phys Chem C 2009;113:1601-5;

(d) Hou J, Park MH, Zhang S, Yao Y, Chen LM, Li JH, Yang Y. Bandgap and molecular energy level control of conjugated polymer photovoltaic materials based on benzo[1,2-b:4,5-b′]dithiophene. Macromolecules 2008;41:6012-8;

(e) Yasuda T, Imase T, Yamamoto T. Synthesis, characterization, and optical and electrochemical

properties of new 2,1,3-benzoselenadiazole-based CT-type copolymers. Macromolecules 2005;38:7378-5;

(f) Yang J, Jiang C, Zhang Y, Yang R, Yang W, Hou Q, Cao Y. High-efficiency saturated red emitting polymers derived from fluorene and naphthoselenadiazole. Macromolecules 2004;37:1211-8.

[6] (a) Uchiyama S, Kimura K, Gota C, Okabe K, Kawamoto K, Inada N, Yoshihara T, Tobita S. Environment-sensitive fluorophores with benzothiadiazole and benzoselenadiazole structures as candidate components of a fluorescent polymeric thermometer. Chem Eur J 2012;18:9552-63;

(b) Das S, Pati PB, Zade SS. Cyclopenta[c]thiophene-based D-A conjugated copolymers: effect of heteroatoms (S, Se, and N) of benzazole acceptors on the properties of polymers. Macromolecules 2012;45:5410-7;

(c) İçli-Özkut M, İpek H, Karabay B, Cihaner A, Önal AM. Furan and benzochalcogenodiazole based multichromic polymers *via* a donor-acceptor approach. Polym Chem 2013;4:2457-63;

(d) Qian G, Abu H, Wang ZY. A precursor strategy for the synthesis of low band-gap polymers: an efficient route to a series of near-infrared electrochromic polymers. J Mater Chem 2011;21:7678-85;

(e) Koyuncu FB, Davis AR, Carter KR. Emissive conjugated polymer networks with tunable band-gaps *via* thiol-ene click chemistry. Chem Mater 2012;24:4410-6;

(f) Chen L, Wang L, Jing X, Wang F. Color tuning of novel 2,1,3-naphthothiadiazole and 2,1,3-benzoselenadiazole based D-A-D' type dopants to realize highly efficient saturated red emission in non-polar solvents. J Mater Chem 2011;21:10265-7.

[7] (a) Coombs BA, Lindner BD, Edkins RM, Rominger F, Beeby A, Bunz UHF. Photophysical property trends for a homologous series of bis-ethynylsubstituted benzochalcogendiazoles. New J. Chem 2012;36:550-3;

(b) Bryant JJ, Lindner BD, Bunz UHF. Water-soluble bis-triazolyl benzochalcogendiazole cycloadducts as tunable metal ion sensors. J Org Chem 2013;78:1038-44.

[8] Li DQ, Li H, Liu MC, Chen JX, Ding JC, Huang XB, Wu HY. Synthesis, optical and electrochemical properties of novel D-π-A type conjugated polymers based on benzo[*c*][1,2,5]selenadiazole unit *via* alkyne module. Polymer 2013;54:6158-64.

[9] Li DQ, Li H, Liu MC, Chen JX, Ding JC, Huang XB, Wu HY. Novel D-π-A conjugated polymer chemosensor based on benzo[c][1,2,5]selenadiazole for highly selective and sensitive recognition of mercury (II) ion. Macromol Chem Phys 2014;215:82-9.

[10] (a) Li DQ, Liu MC, Chen JX, Lan J, Huang XB, Wu HY. Synthesis and photoelectric properties of novel indeno[2,1-*a*]phenalene-based derivatives. Dyes Pigm 2013;97:389-96;

(b) Huang XB, Zeng LT, Zeng ZB, Wu JS. Intramolecular domino electrophilic and thermal cyclization of *peri*-ethynylene naphthalene oligomers. Chem Eur J 2011;17:14907-15.

[11] Tsubata Y, Suzuki T, Myashi T. Single-component organic conductors based on neutral radicals containing the pyrazino-TCNQ skeleton. J Org Chem 1992;57:6749-55.

[12] Vieira AA, Cristiano R, Bortoluzzi AJ, Gallardo H. Luminescent 2,1,3-benzothiadiazole-based liquid crystalline compounds. J Mol Struct 2008;875:364-71.

[13] Misra R, Gautam P, Sharma R, Mobin SM. Donor-π-acceptor-π-donor ferrocenyl benzothiadiazoles: synthesis, structure, and properties. Tetrahedron Lett 2013;54:381-3.

[14] Lin W, Yuan L, Cao Z, Feng J, Feng Y. Fluorescence enhancement of coumarin-quinoline by transition metal ions: Detection of paramagnetic Ni^{2+} and Co^{2+}. Dyes Pigm. 2009;83:14-20.

[15] (a) Neto BAD, Lopes ASA, Ebeling G, Gonçalves RS, Costa VEU, Quina FH, Dupont J. Photophysical and electrochemical properties of π-extended molecular 2,1,3-benzothiadiazoles. Tetrahedron 2005;61:10975-82;

(b) Agou T, Kojima T, Kobayashi J, Kawashima T. Synthesis of π-conjugated dendrimers based on azaborines. Org Lett 2009;11:3534-7.

[16] (a) Do J, Huh J, Kim E. Solvatochromic fluorescence of piperazine-modified bipyridazines for an organic solvent-sensitive film. Langmuir 2009;25:9405-12;

(b) Chen CT, Liao SY, K. Lin J, Lai LL. Syntheses, charge distribution, and molecular second-order nonlinear optical properties of push-pull bisdithiolene nickel complexes. Adv Mater 1998;10:334-8.

[17] Reichardt C. Solvatochromic dyes as solvent polarity indicators. Chem Rev 1994;94:2319-58.

[18] Gilani AG, Moghadam M, Zakerhamidi MS, Moradi E. Dyes Pigm. 2012;92:1320-30.

[19] Lakowicz JR. Principles of fluorescence spectroscopy, Plenum Press, New York, 1983, p.190.

[20] (a) Yang SW, Elangovan A, Hwang KC, Ho TI. Electronic polarization reversal and excited state intramolecular charge transfer in donor/acceptor ethynylpyrenes. J Phys Chem B 2005;109:16628-35;

(b) Feng J, Chen X, Han Q, Wang H, Lu P, Wang Y. Naphthalene-based fluorophores: synthesis characterization, and photophysical properties. J Lumin 2011;131:2775-83;

(c) Cao D, Liu Z, Zhang G, Li G. The synthesis, photophysical properties and fluoride anion recognition of a novel branched organoboron compound. Dyes Pigm 2009;81:193-6.

[21] Kamlet MJ, Abboud JLM, Abraham MH, Taft RW. Linear salvation energy relationships. 23. A comprehensive collection of the solvatochromic parameters, π*, α, and β, and some methods for simplifying the generalized solvatochromic equation. J Org Chem 1983;48:2877-87.

[22] Frisch MJ, Trucks GW, Schlegel HB, Scuseria GE, Robb MA, Cheeseman JR, et al. Gaussian 03, revision C.02. Wallingford, CT: Gaussian, Inc.; 2004.

[23] Zhang Y, Murphy CB, Jones WE. Poly[*p*-(phenyleneethynylene)-*alt*- (thienyleneethynylene)] polymers with oligopyridine pendant groups: highly sensitive chemosensors for transition metal ions. Macromolecules 2002;35:630-6.

[24] Zou Y, Wan M, Sang G, Ye M, Li Y. An alternative copolymer of carbazole and thieno[3,4b]pyrazine: synthesis and mercury detection. Adv Funct Mater 2008;18:2724-32.

[25] Yuan D, Brown RG. Enhanced nonradiative decay in aqueous solutions of aminonaphthalimide derivatives *via* water-cluster formation. J. Phys Chem A 1997;101:3461-6.

Figure Captions

Fig. 1. TGA curves of compounds **7a-i**.

Fig. 2. UV-vis absorption spectra of compounds **7a-i** (1×10^{-5} mol/L in $CHCl_3$).

Fig. 3. Fluorescence spectra of compounds **7a-i** in $CHCl_3$.

Fig. 4. Fluorescence photos of **7a-i** in $CHCl_3$ under a 365 nm UV lamp.

Fig. 5. UV-vis spectra of **7c** in various solvents.

Fig. 6. Fluorescence spectra of **7c** in various solvents.

Fig. 7. Fluorescence photos of **7c** in different solvents under a 365 nm UV lamp: from left to right: toluene, $CHCl_3$, THF, DCM, DMF, Acetone and CH_3CN.

Fig. 8. Polt of emission maxima of **7c** *vs* $E_T(30)$ solvent polarity parameter of various solvents.

Fig. 9. Polt of Stokes shifts ($\Delta\nu$) of **7c** *vs* orientation polarizability (Δf) of various solvents.

Fig. 10. Plots of the measured and calculated emission maxima (a) and Stokes shifts (b) for **7c** obtained by the Kamlet-Taft equation.

Fig. 11. Molecular orbital diagrams for the LUMO (up) and HOMO (down) of compounds **7a-i** from DFT calculations.

Fig. 12. Comparison of experimental optical energy gaps (from UV-vis spectra) with theoretical values.

Fig. 13. Fluorescence spectra of **7c** (1.0×10^{-5} mol L^{-1}) in THF with increasing concentration of Hg^{2+} (0, 0.2, 0.4, 0.6, 0.8, 1.0, 1.5, 2.0, 2.5, 3.0, 3.5, 4.0, 4.5×10^{-5} mol·L^{-1} in CH_3CN) (λ_{ex} = 458 nm). Inset: visible fluorescence of **7c** before (left) and after (right) the addition of Hg^{2+} (4.0×10^{-5} mol·L^{-1}) under a 365 nm UV lamp.

Fig. 14. Calibration curve was obtained from the plot of fluorescence intensity of **7c** with the added Hg^{2+} from 0 to 4.5×10^{-5} mol·L^{-1}.

Fig. 15. Stern-Volmer plots of **7c** emission quenched by Hg^{2+}. Inset: a linear Stern-Volmer plot was obtained at low concentrations of Hg^{2+} (0 to 1.0×10^{-5} mol·L^{-1}).

Fig. 16. Fluorescence quenching degree of **7c** (1.0×10^{-5} mol·L^{-1}) in the presence of Hg^{2+} (4.0×10^{-5} mol·L^{-1}) and other metal ions (each 4.0×10^{-5} mol·L^{-1}).

Fig. 17. Metal specificity: the concentration of **7c** was 1.0×10^{-5} mol·L^{-1}, the concentration of Hg^{2+} was 4.0×10^{-5} mol·L^{-1} and the other metal ions were used at 4.0×10^{-4} mol·L^{-1}. Mix: the mixture of K^{+}, Pb^{2+}, Cu^{2+}, Co^{2+}, Cd^{2+}, Fe^{3+}, Mn^{2+}, Ni^{2+}, Zn^{2+} and Ag^{+}.

Fig. 18. Fluorescence spectra of **7d** (1.0×10^{-5} mol·L^{-1}) in anhydrous THF with increasing water content (0, 0.033, 0.067, 0.1, 0.133, 0.167, 0.233, 0.333, 0.5, 0.667, 0.083, 1, 1.17, 1.5, 1.83%, v/v) (λ_{ex} = 502 nm, slit width (EX/EM): 5 nm/5 nm). Inset: Visible fluorescence of **7d** before (left) and after (right) the addition of water (water content: 1.83%) under a 365 nm UV lamp.

Fig. 19. Fluorescence intensity of **7d** *vs* the water content.

Fig. 20. Stern-Volmer plot of **7d** in THF emission quenched by water.

Scheme 1. Synthesis procedures of **BSe** derivatives **7a-i**.

Table Captions

Table 1. Photophysical properties of compounds **7a-i** in $CHCl_3$.

Table 2. UV-vis absorption maxima and fluorescence emission maxima of **7c** and solvent polarity parameter in different solvents.

Table 1. Photophysical properties of compounds **7a-i** in $CHCl_3$.

Compound	λ_{abs}^{max} (nm)	λ_{em}^{max} (λ_{ex}) (nm)	Stoke's shift (nm)	E_g^{op} (eV) [a]	HOMO (eV) [b]	LUMO (eV) [b]	E_g (eV) [b]	Φ_{PL} [c]
6	393	464(373)	71	2.85	-	-	-	-
7a	444	546(448)	102	2.48	-5.65	-3.08	2.57	0.20
7b	452	563(450)	111	2.42	-5.50	-2.99	2.51	0.37
7c	465	595(460)	130	2.34	-5.29	-2.90	2.39	0.17
7d	488	669(489)	181	2.20	-4.86	-2.65	2.21	0.04
7e	443	546(445)	103	2.48	-5.77	-3.21	2.56	0.25
7f	443	543(446)	100	2.49	-5.90	-3.32	2.58	0.27
7g	429	527(438)	98	2.55	-6.18	-3.60	2.58	0.31
7h	432	518(434)	86	2.57	-6.17	-3.52	2.65	0.22
7i	435	512(428)	77	2.53	-5.87	-3.17	2.70	0.27

[a] E_g^{op} was calculated from the absorption of UV-vis spectra: band gap energy [eV] = 1240/wavelength [nm].

[b] DFT quantum mechanical calculations (B3LYP/6-31+G**).

[c] Quantum yields were determined with the quinine sulfate solution as a fluorescence reference (Φ_r = 0.55 in 0.5 mol/L H_2SO_4).

Table 2. UV-vis absorption maxima and fluorescence emission maxima of **7c** and solvent polarity parameter in different solvents.

	Toluene	$CHCl_3$	THF	DCM	DMF	Acetone	CH_3CN
λ_{abs}/nm	459	465	457	460	455	452	451
ν_{abs}/cm^{-1}	21786	21505	21882	21739	21978	22124	22173
λ_{em}/nm	553	584	575	586	604	583	604
ν_{em}/cm^{-1}	18083	16807	17391	17065	16556	17153	16556
ν_{em}/cm^{-1} [a]	18088	16834	17443	17041	16570	17040	16588
$\Delta\nu$/cm^{-1}	3703	4698	4491	4674	5422	4971	5617
$\Delta\nu$/cm^{-1} [a]	3610	4906	4619	4611	5409	4985	5436
Δf	0.0135	0.155	0.210	0.218	0.276	0.284	0.305
$E_T(30)$/kcal mol^{-1} [b]	33.9	39.1	37.4	40.7	43.2	42.2	45.6

[a] Obtained by the Kamlet-Taft equation.

[b] The values were taken from the reference [18].

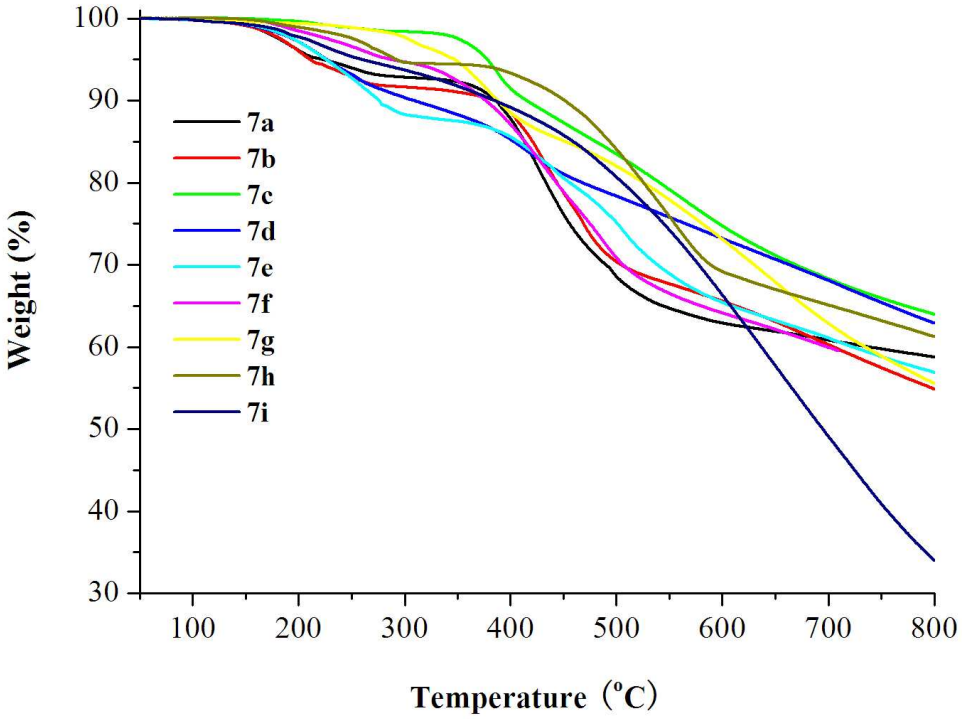

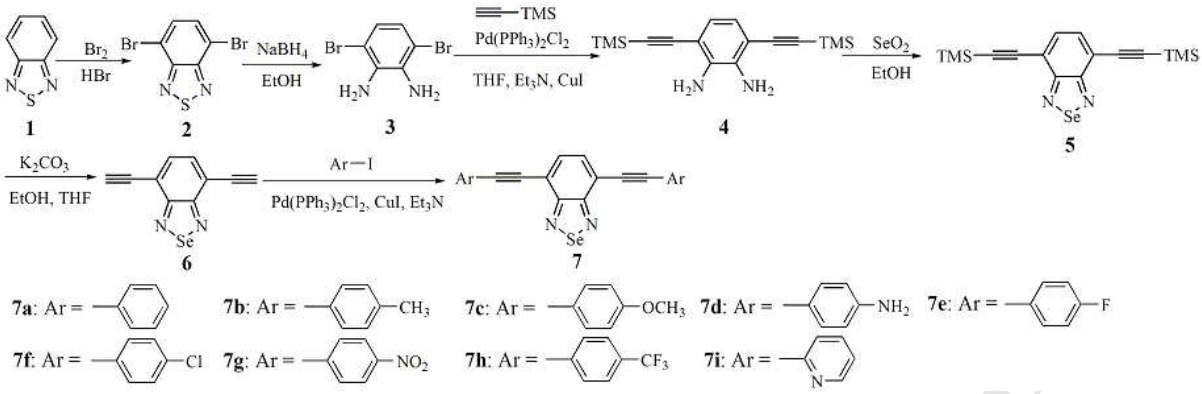

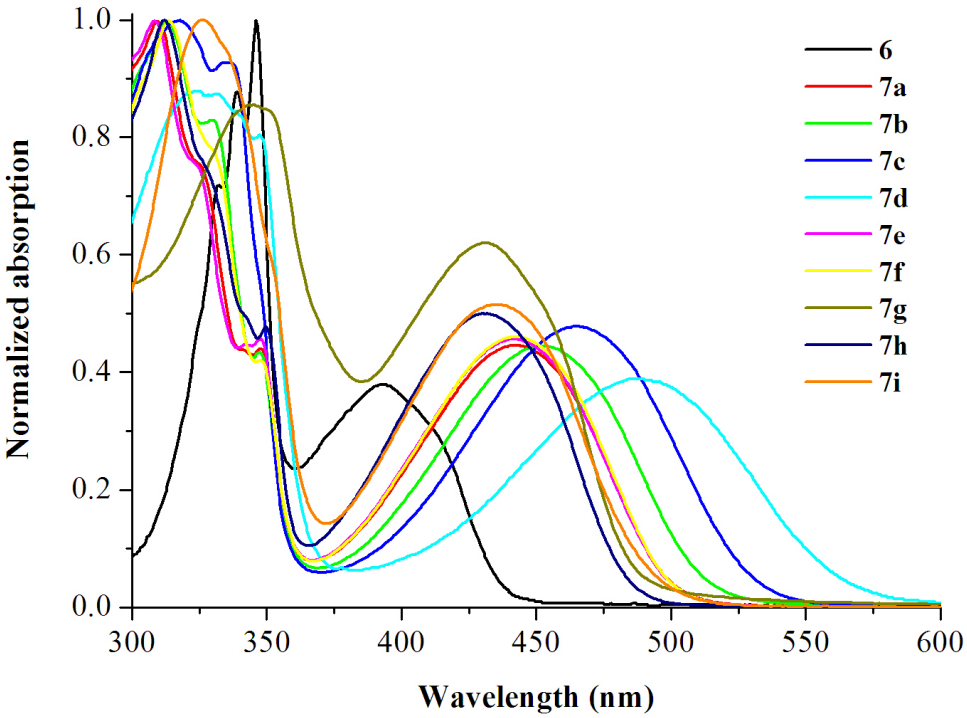

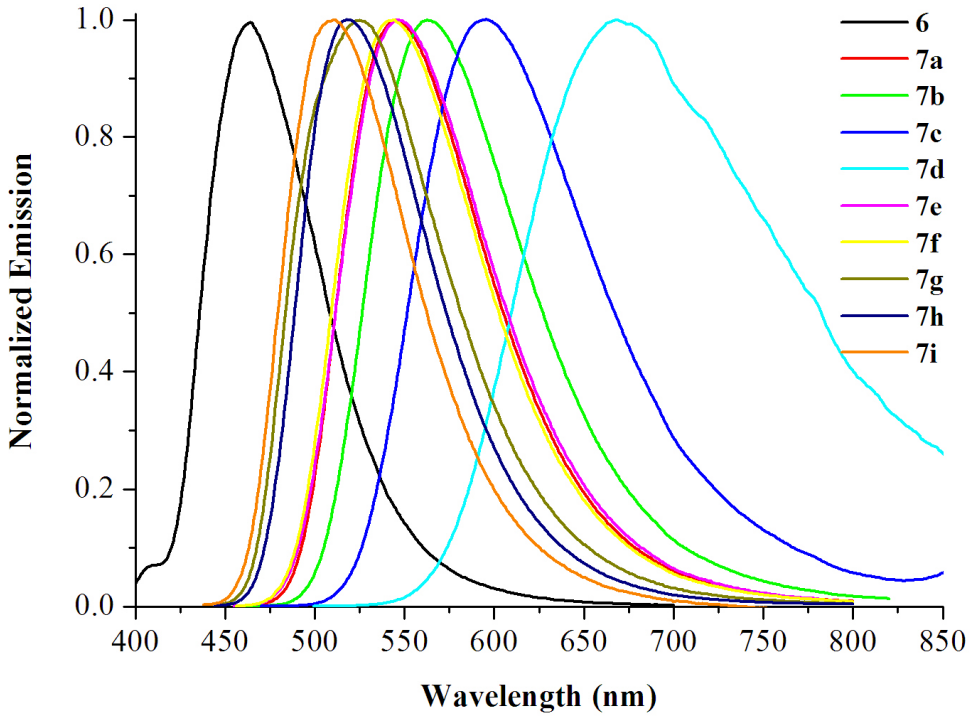

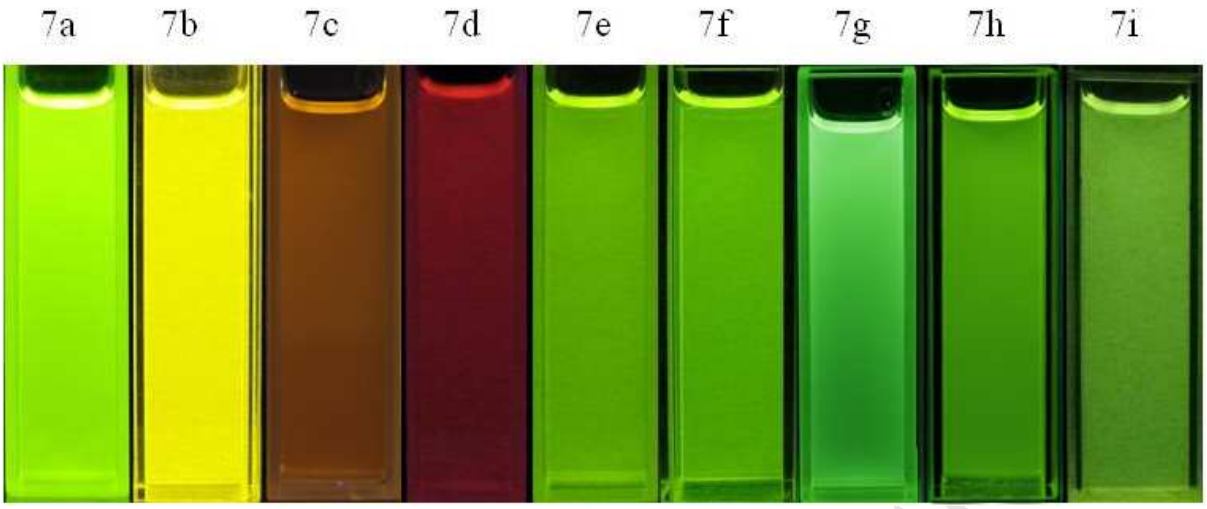

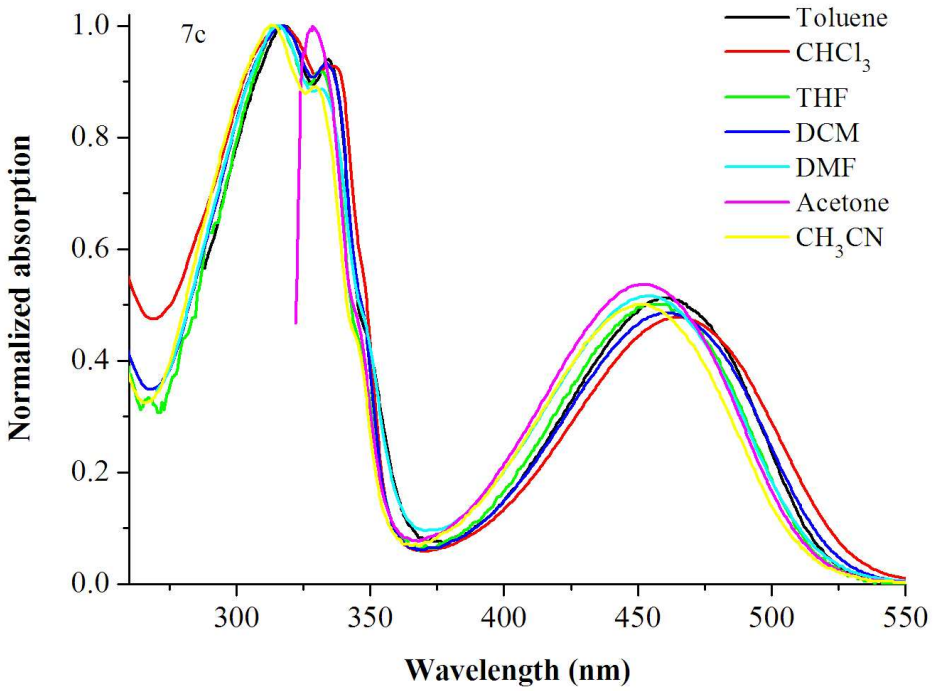

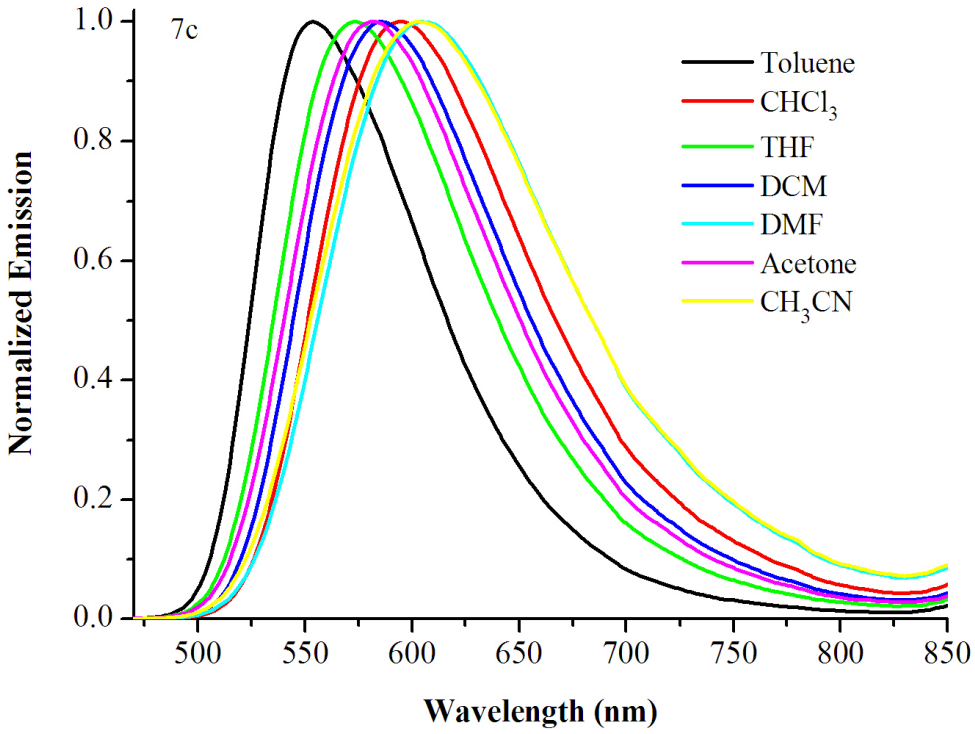

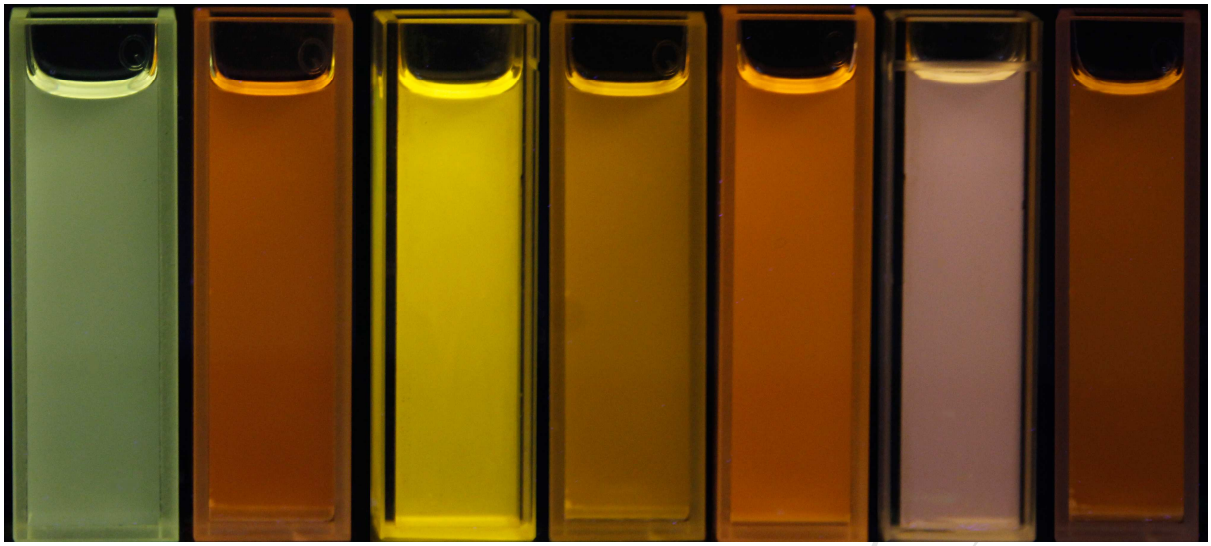

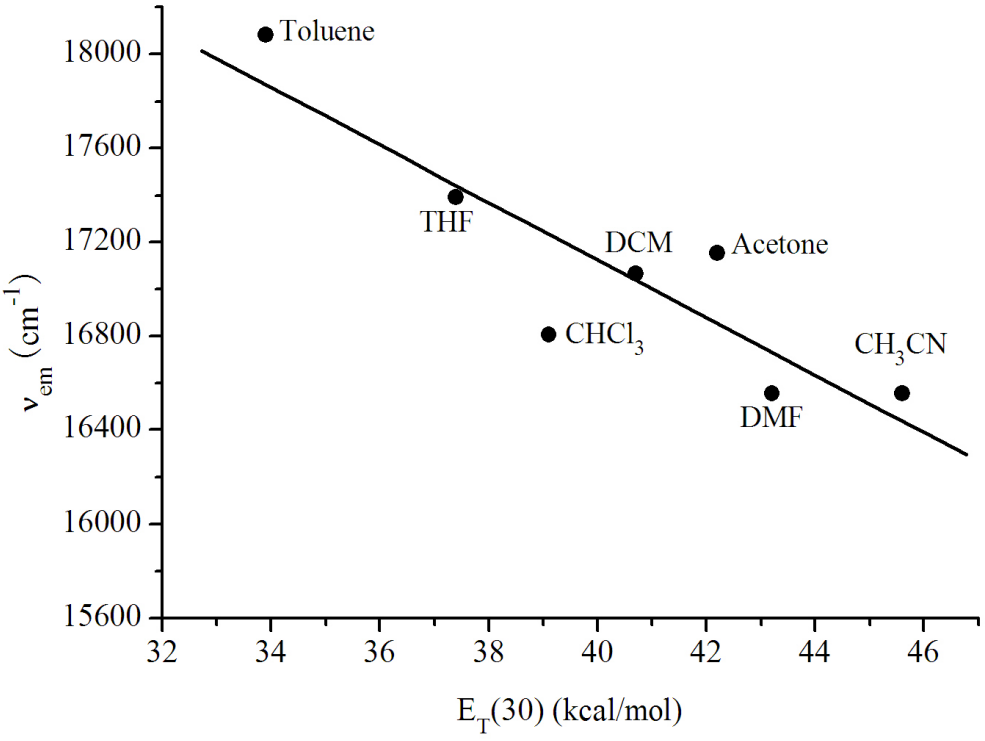

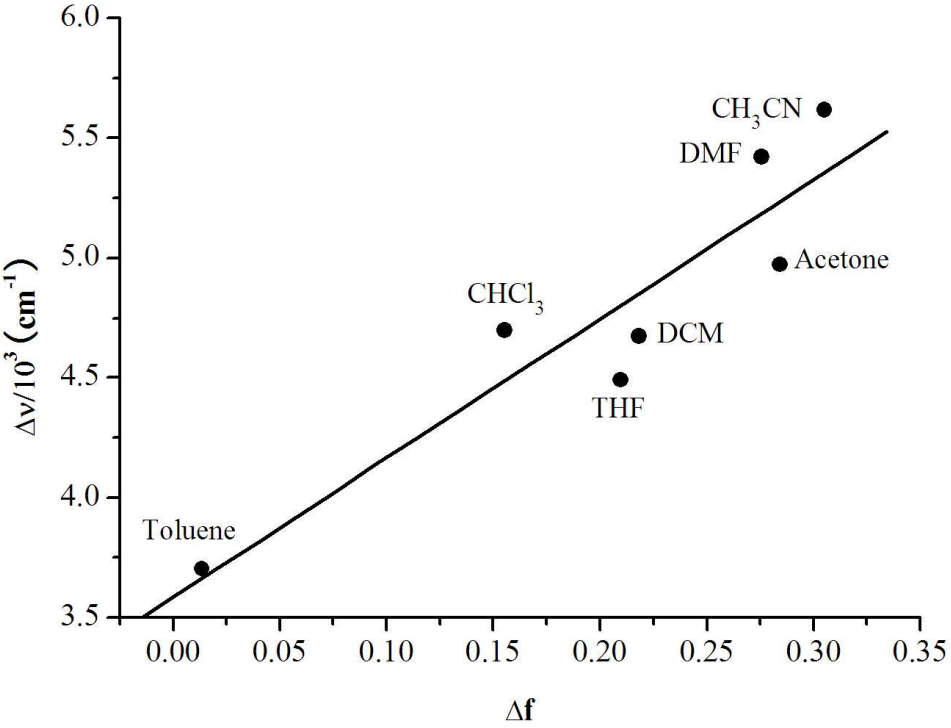

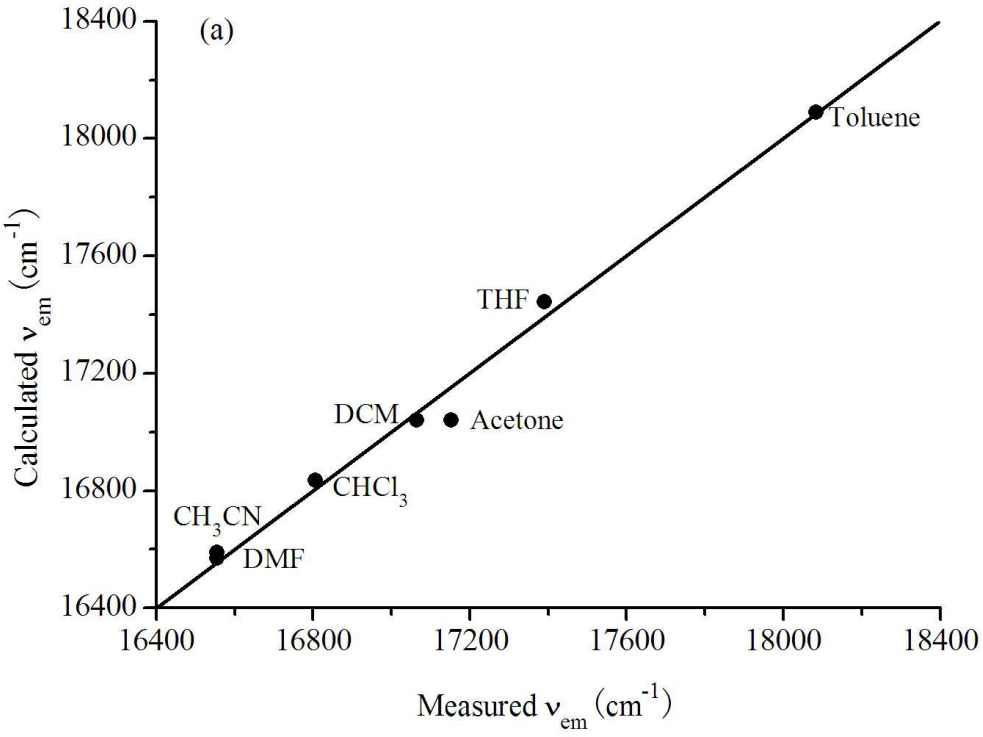

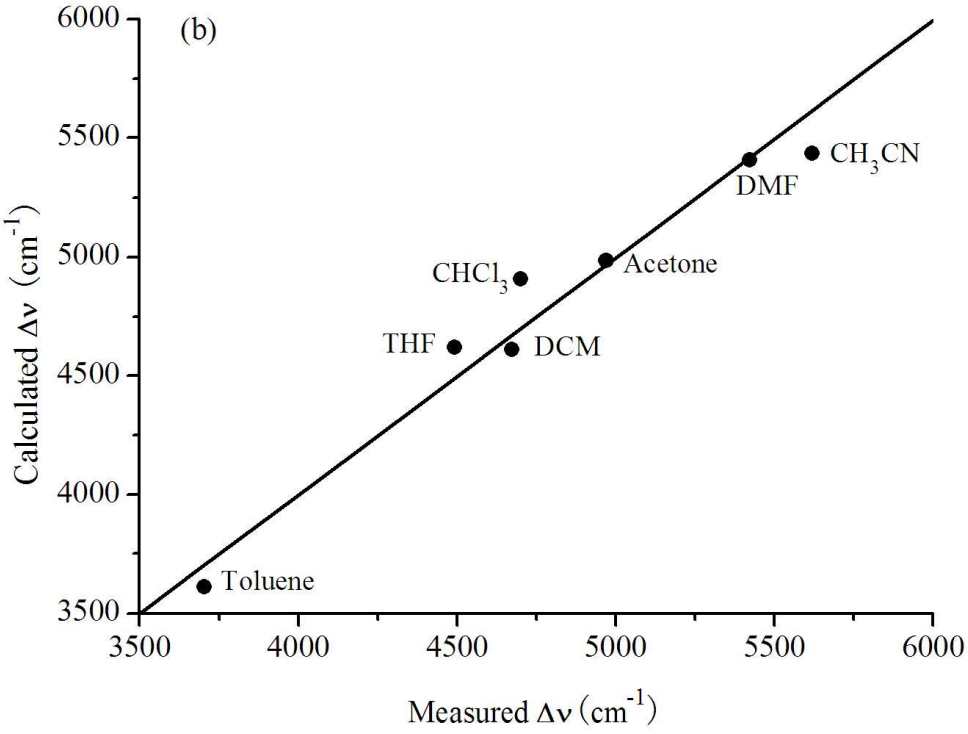

7a	7b	7c
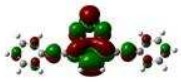		
		
7d	**7e**	**7f**
		
		
7g	**7h**	**7i**
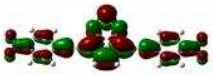		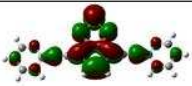
		

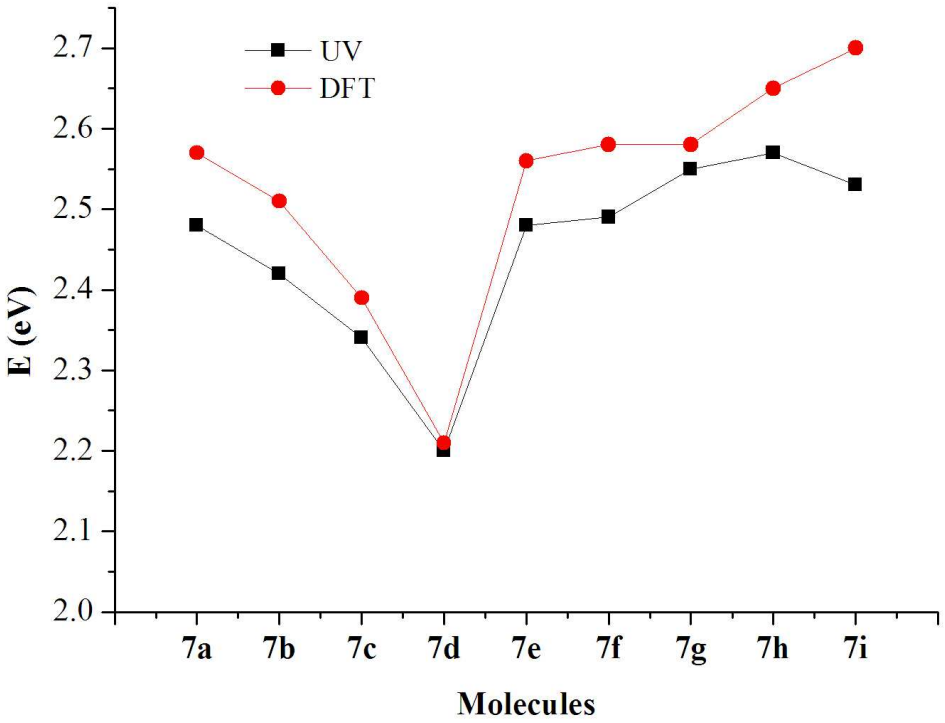

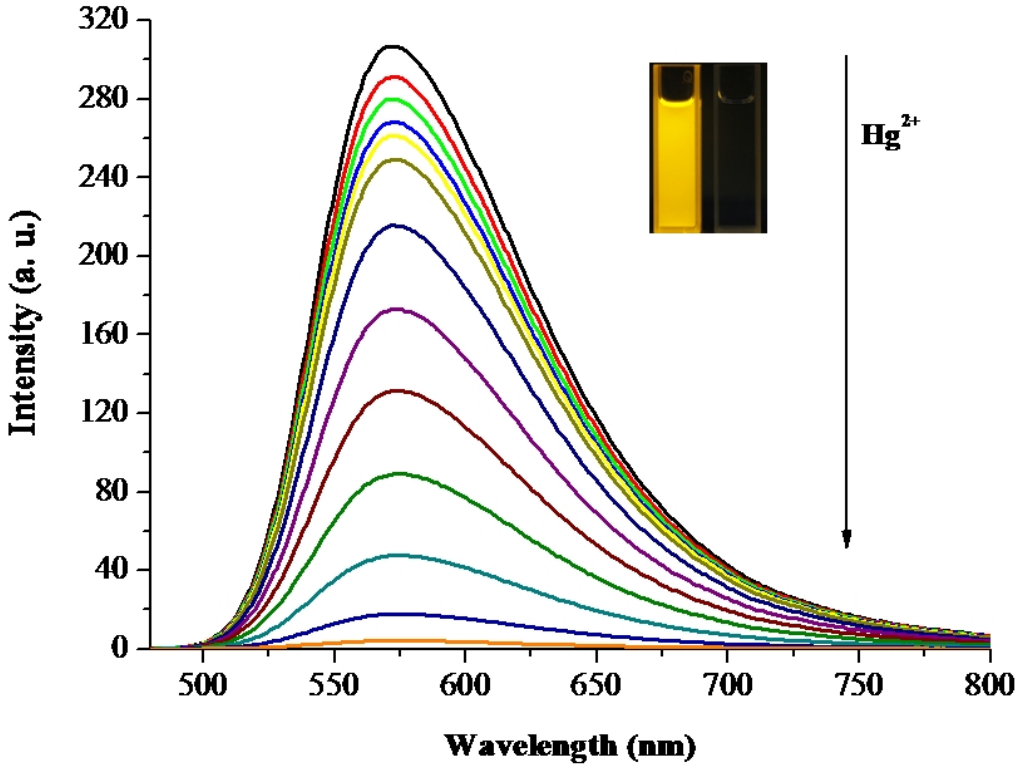

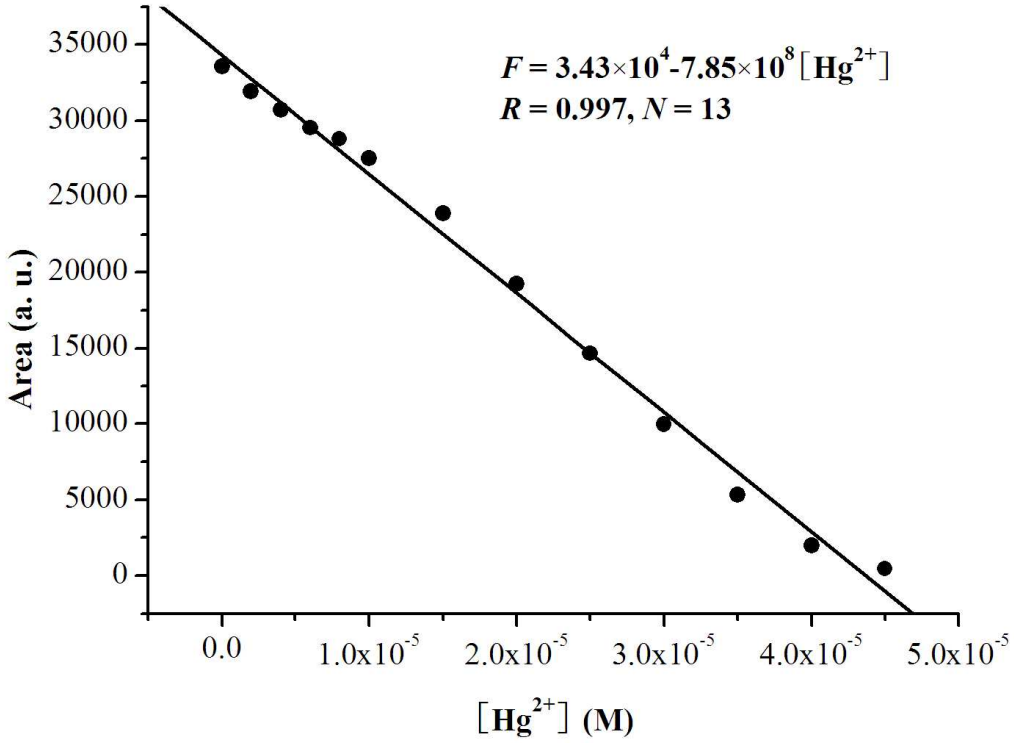

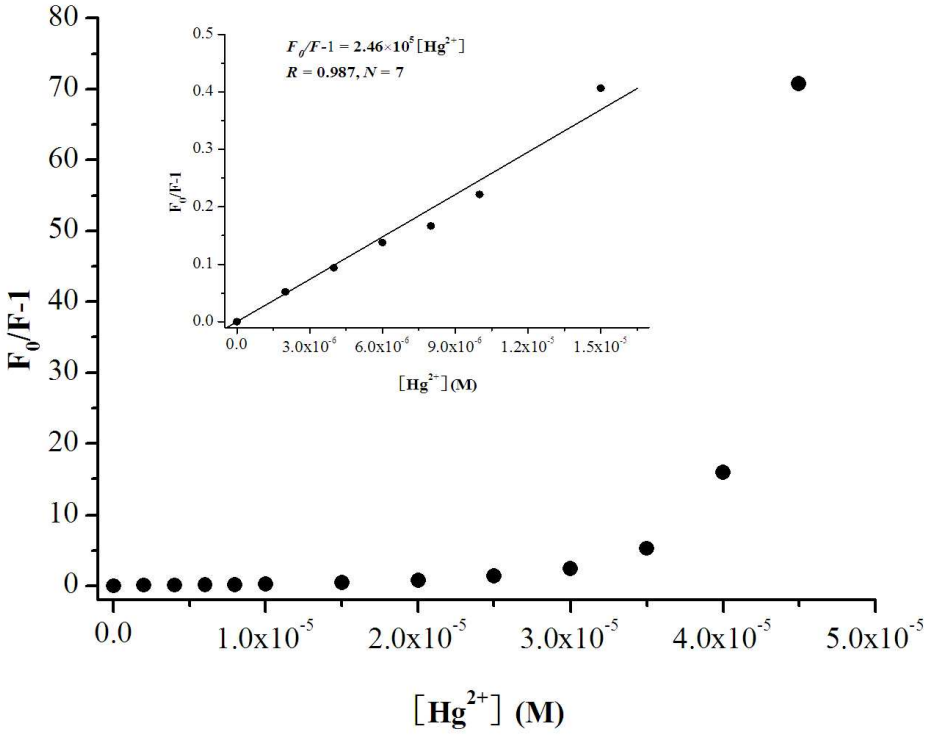

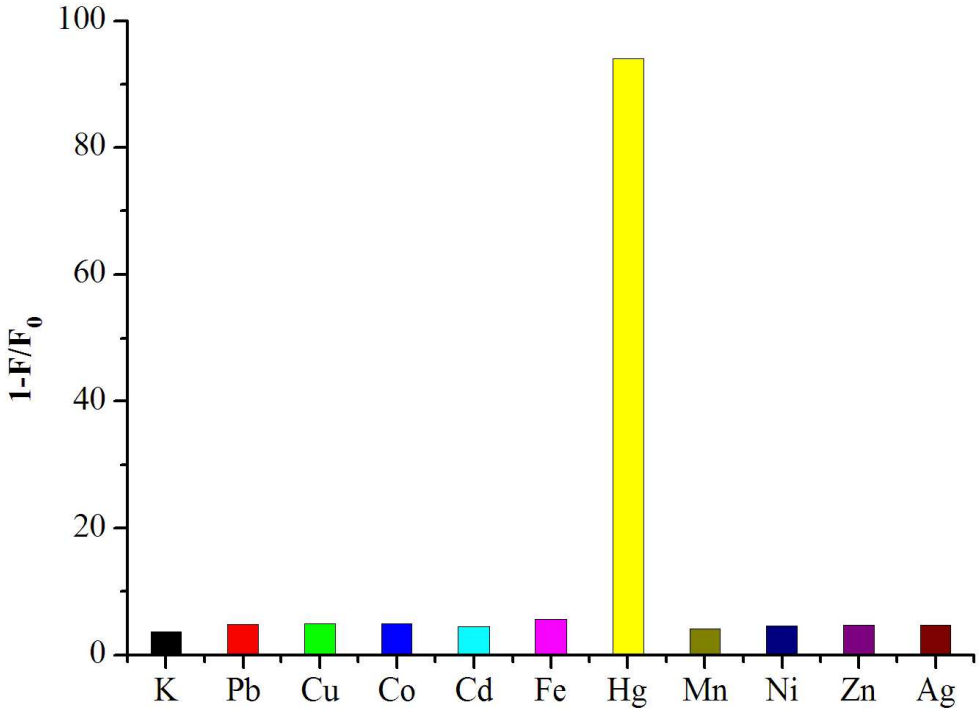

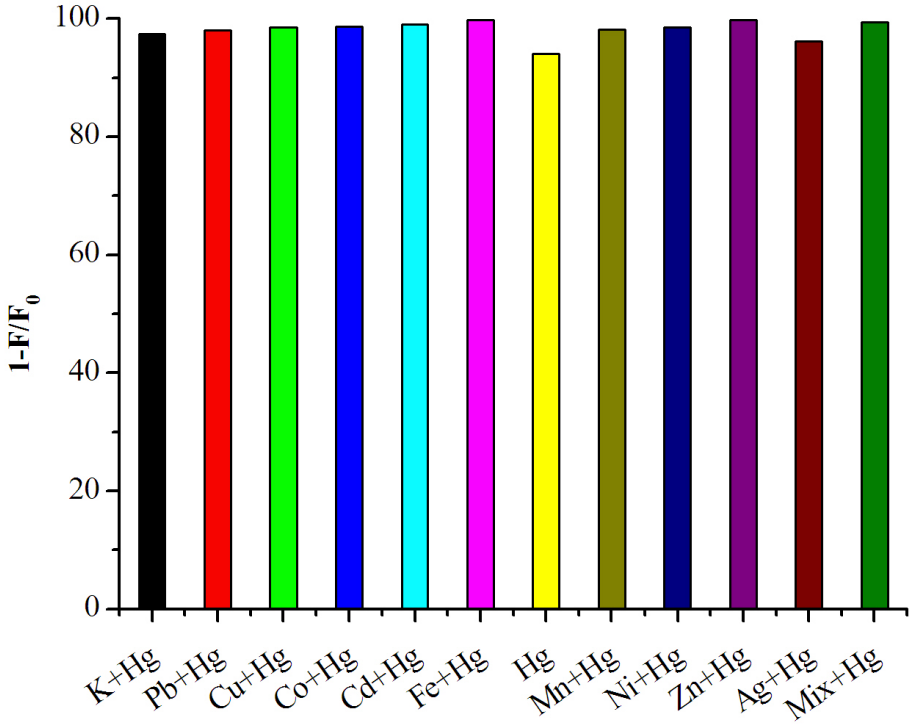

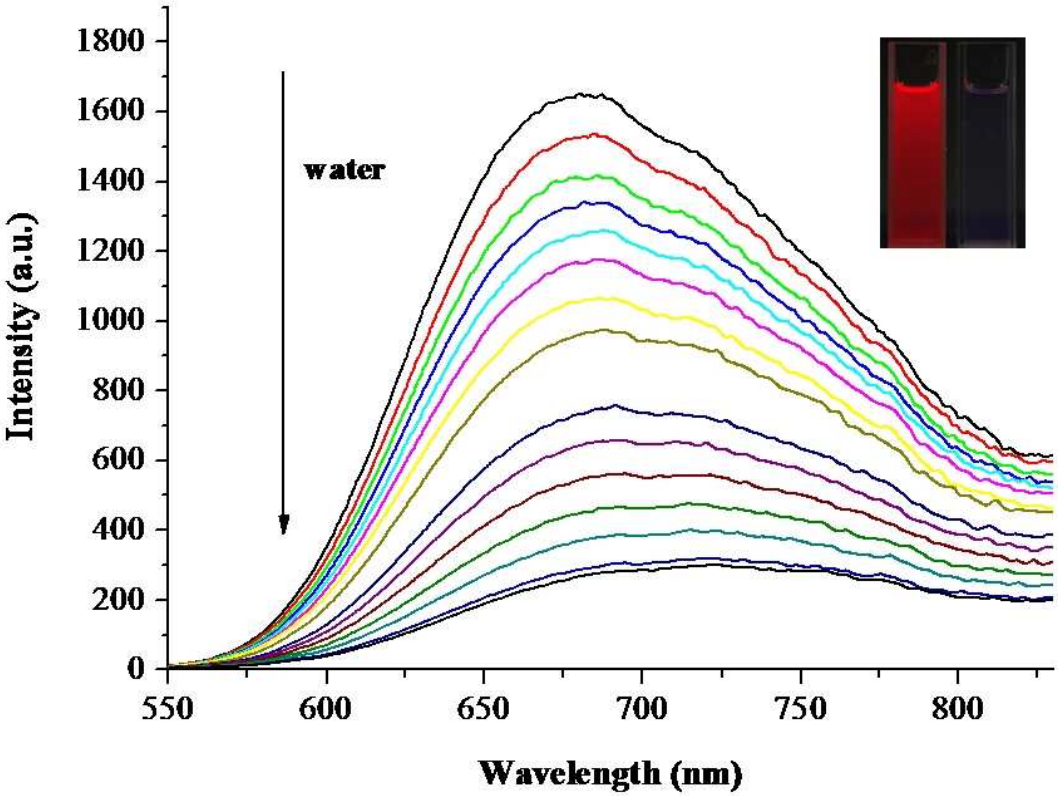

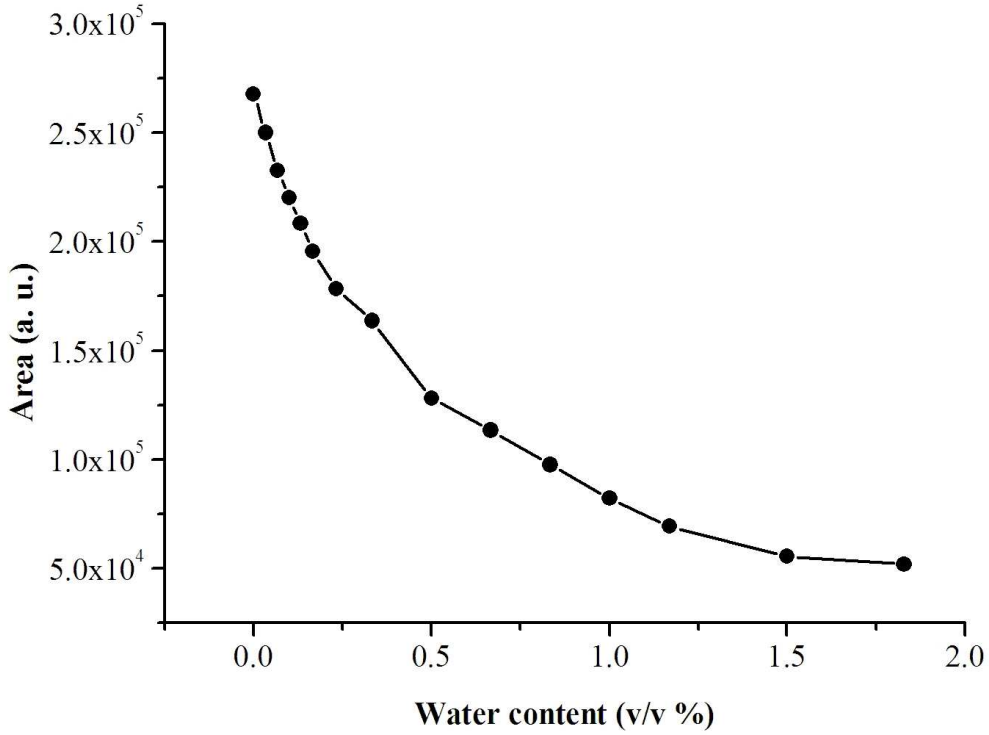

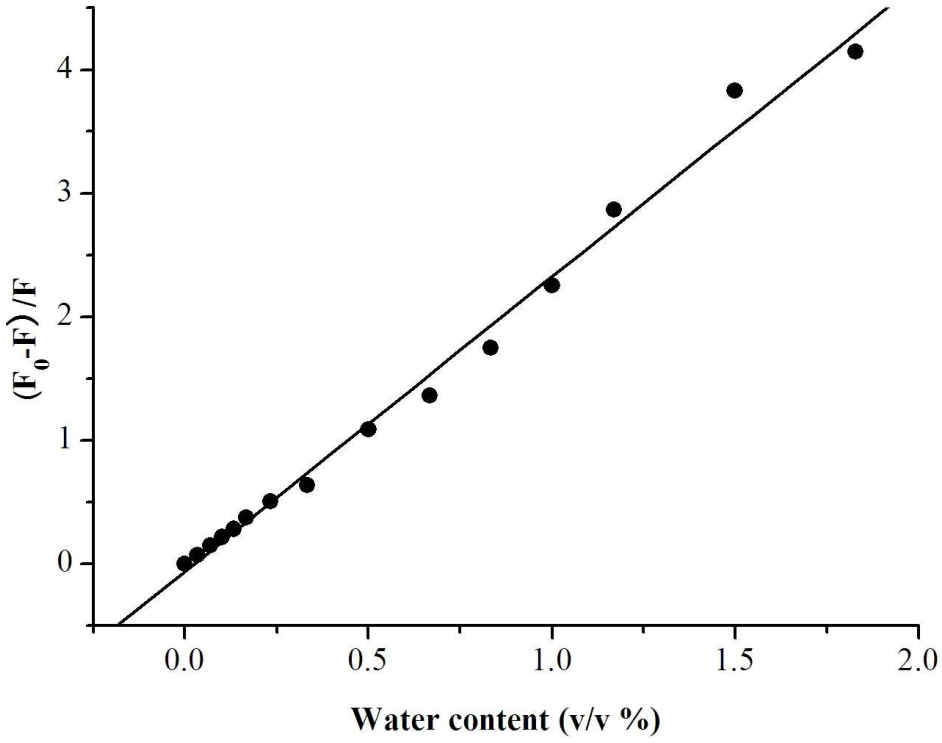

Highlights:

► Synthesis and characterization of novel D-π-A benzo[*c*][1,2,5]selenadiazole-based derivatives.

► The new compounds exhibit positive solvatochromism.

► The band gaps of the new compounds are in the range of 2.21-2.70 eV.

► Application as fluorescent sensors using benzo[c][1,2,5]selenadiazole as an acceptor or a fluorophore.

Supporting Information

D-π-A benzo[*c*][1,2,5]selenadiazole-based derivatives *via* an ethynyl bridge: photophysical properties, solvatochromism and applications as fluorescent sensors

Hui Li[a], Yang Guo[b], Yunxiang Lei[a], Wenxia Gao[a], Miaochang Liu[a], Jiuxi Chen[a], Yuefei Hu[c], Xiaobo Huang[a,*], Huayue Wu[a,*]

[a]College of Chemistry and Materials Engineering, Wenzhou University, Wenzhou 325035, P. R. China

[b]School of Chemistry and Chemical Engineering, Nanjing University, Nanjing, 210093, P. R. China

[c]Department of Chemistry, Tsinghua University, Beijing 100084, P. R. China

*Corresponding authors. Tel.: +86 577 88368280; fax: +86 577 88368280

E-mail addresses: xiaobhuang@wzu.edu.cn (X. Huang); huayuewu@wzu.edu.cn (H. Wu)

Contents:

1. The optical properties of 7a-i (except 7c)

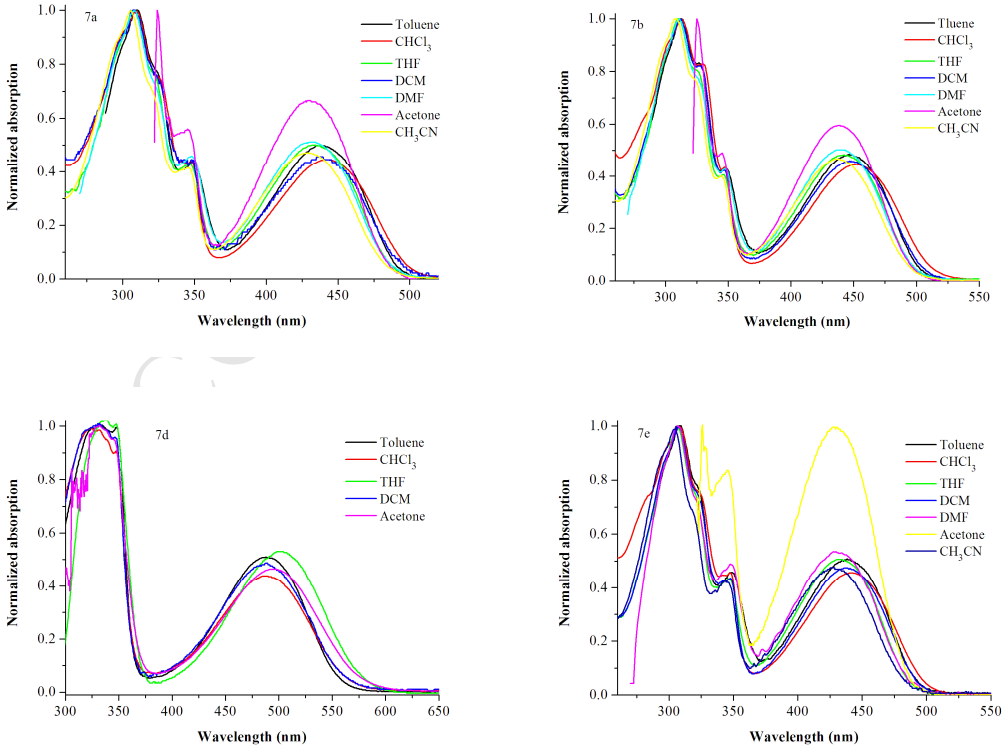

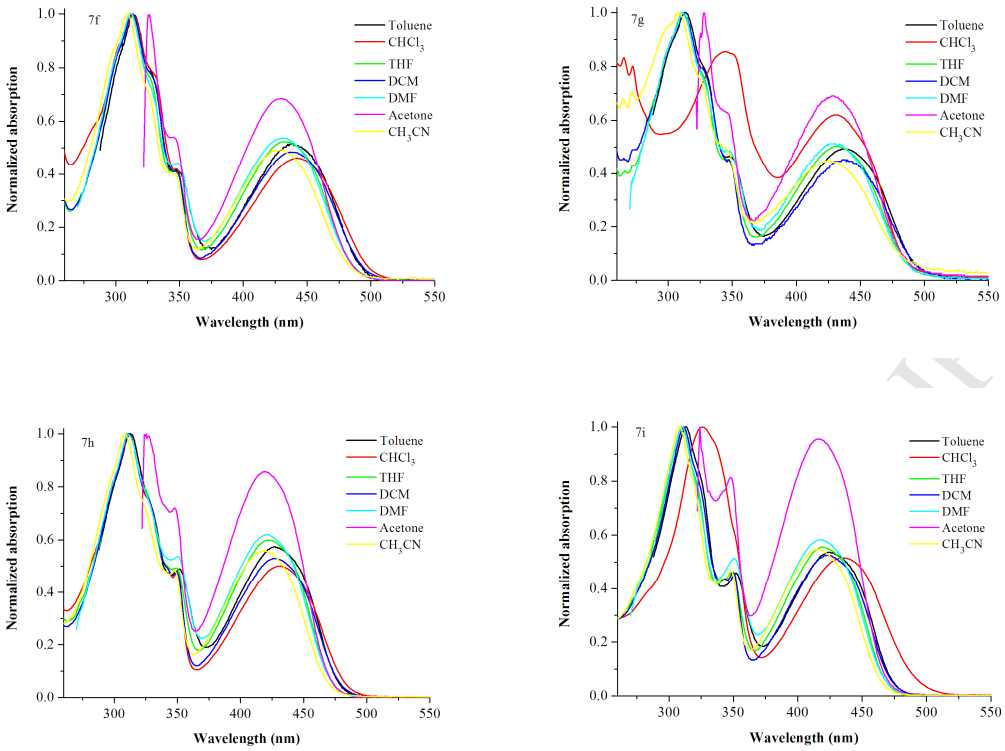

Fig. S1. UV-vis absorption spectra of **7a-i** (except **7c**) in various solvents.

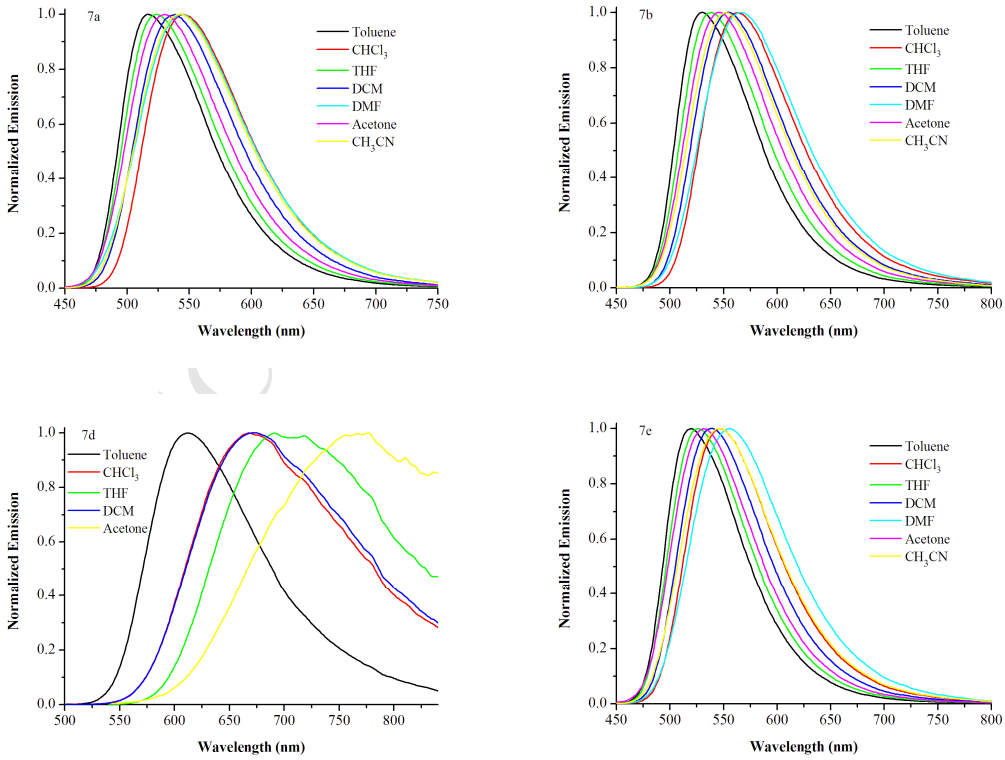

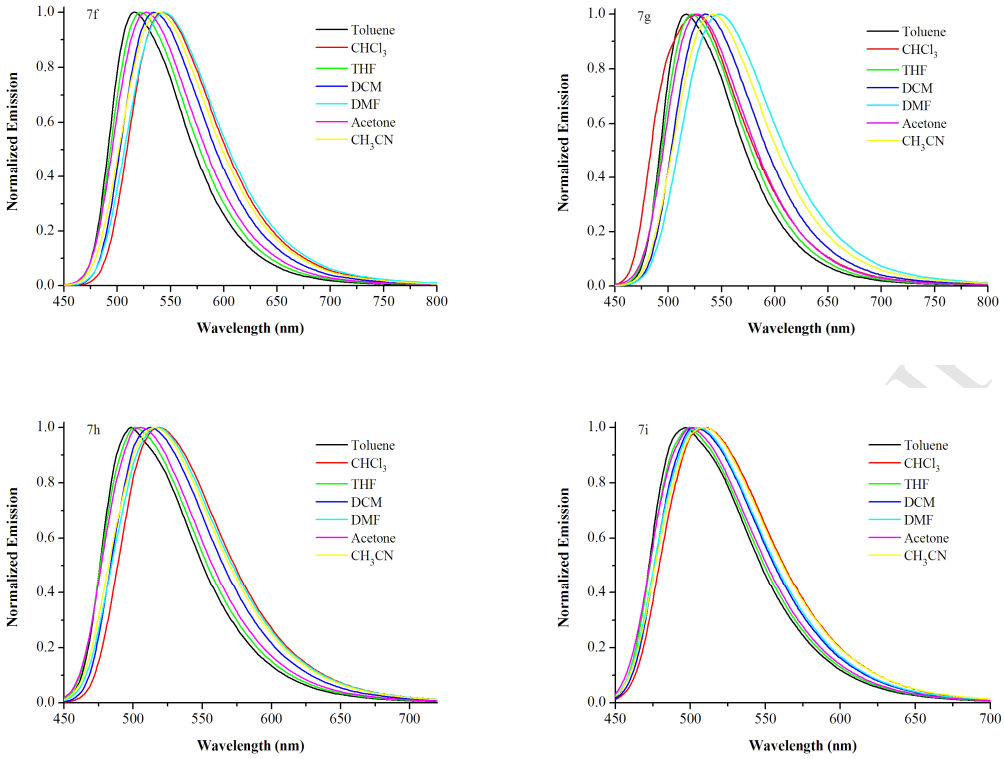

Fig. S2. Fluorescence spectra of compounds **7a-i** (except **7c**) in various solvents.

Table S1. The maximum absorption wavelengths (λ_{abs}^{max}) of **7a-i** (except **7c**) in different solvents.

	Toluene	$CHCl_3$	THF	DCM	DMF	Acetone	CH_3CN
7a	438	444	434	437	431	432	429
7b	447	452	442	446	440	439	437
7d	488	488	502	489	509	495	487
7e	439	443	432	437	432	428	428
7f	437	443	432	438	431	430	430
7g	439	429	432	437	427	427	424
7h	425	432	423	428	420	419	419
7i	425	435	420	424	418	416	416

Table S2. The maximum emission wavelengths (λ_{em}^{max}) of **7a-i** (except **7c**) in different solvents.

	Toluene	$CHCl_3$	THF	DCM	DMF	Acetone	CH_3CN
7a	517	546	523	539	544	530	543
7b	530	563	539	555	566	544	552
7d	610	669	689	671	-	767	-
7e	519	546	526	539	555	531	544
7f	516	543	522	535	544	528	539
7g	516	527	523	535	541	528	542
7h	498	518	500	513	517	505	516
7i	497	512	500	503	506	500	509

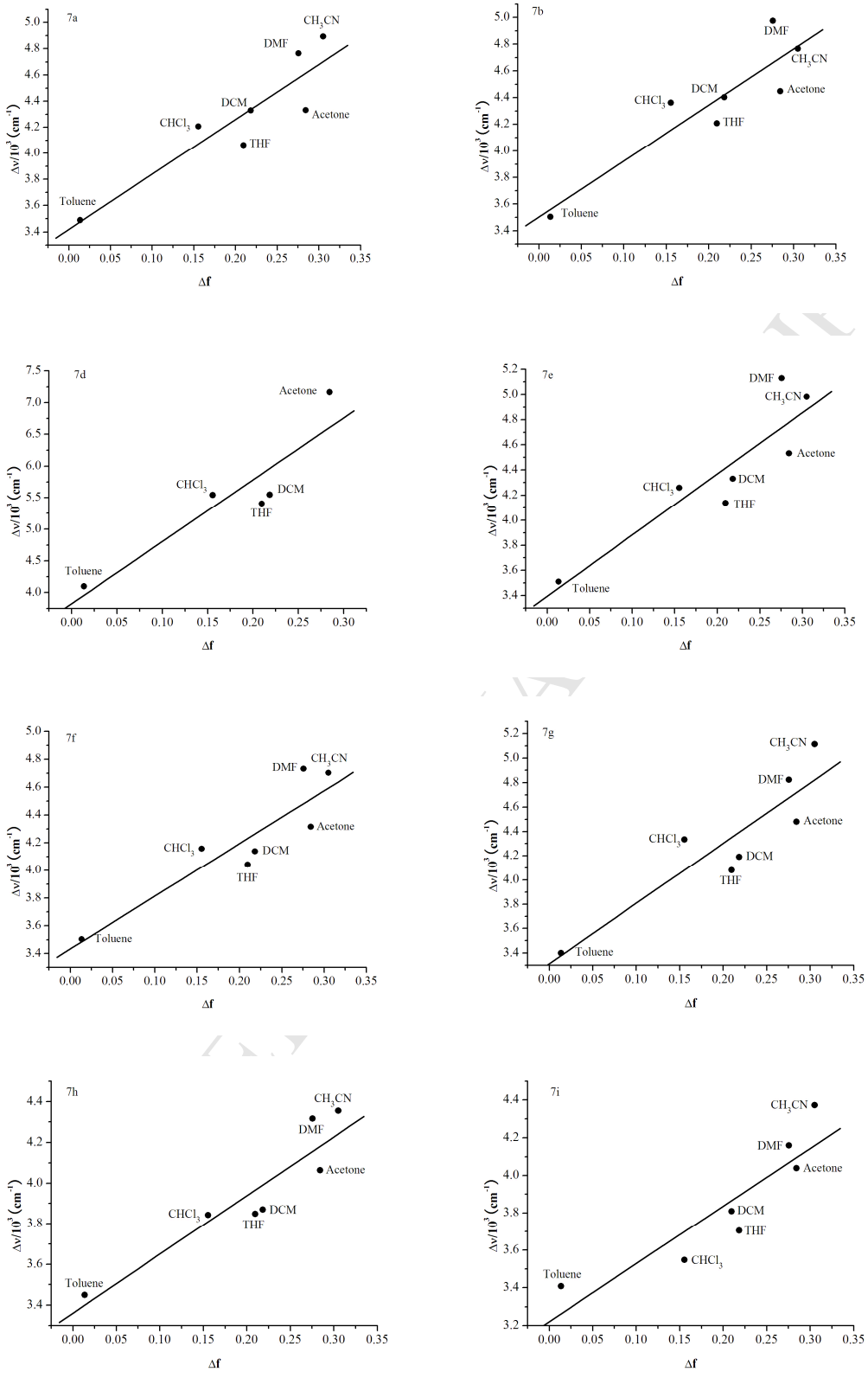

Fig. S3. Polts of Stokes shifts (Δ*v*) of **7a-i** (except **7c**) *vs* orientation polarizability (Δ*f*) of various solvents.

2. Fluorescence responsive behaviors of 7c on various metal ions

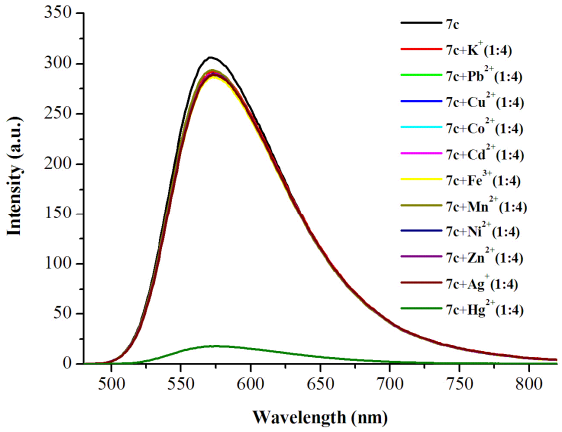

Fig. S4. Fluorescence spectra of **7c** (1.0×10^{-5} mol·L^{-1}) in THF in the presence of Hg^{2+} (4.0×10^{-5} mol·L^{-1}) and other metal ions, such as K^+, Pb^{2+}, Cu^{2+}, Co^{2+}, Cd^{2+}, Fe^{3+}, Mn^{2+}, Ni^{2+}, Zn^{2+} and Ag^+ (each 4.0×10^{-5} mol·L^{-1}) in CH_3CN (λ_{ex} = 458 nm).

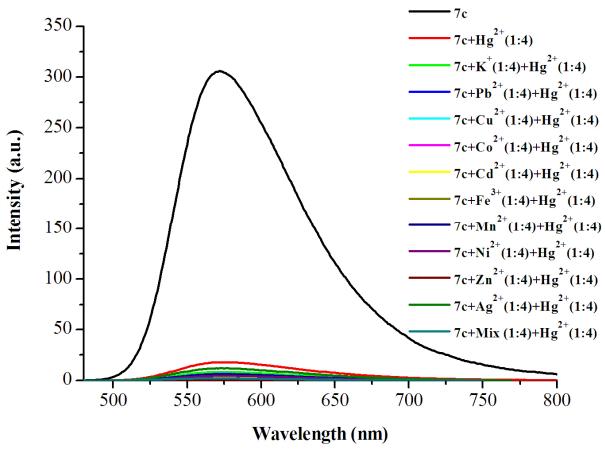

Fig. S5. Metal specificity: the concentration of **7c** is 1.0×10^{-5} mol·L^{-1}, the concentration of Hg^{2+} is 4.0×10^{-5} mol·L^{-1} and the other metal ions are used at 4.0×10^{-5} mol·L^{-1}. Mix: the mixture of K^+, Pb^{2+}, Cu^{2+}, Co^{2+}, Cd^{2+}, Fe^{3+}, Mn^{2+}, Ni^{2+}, Zn^{2+} and Ag^+.

Table S3. The α, β and π* solvent parameters used for constructing Fig. 10 in the main text using the Kamlet-Taft equation. The values were taken from ref. 17 of the main article.

	α	β	π*
Toluene	0	0.11	0.49
$CHCl_3$	0.2	0.1	0.69
THF	0	0.55	0.55
DCM	0.13	0.1	0.73
DMF	0	0.69	0.88
Acetone	0.08	0.48	0.62
CH_3CN	0.19	0.40	0.66

3. ^{1}H NMR, ^{13}C NMR spectra and mass spectra of 7a-i

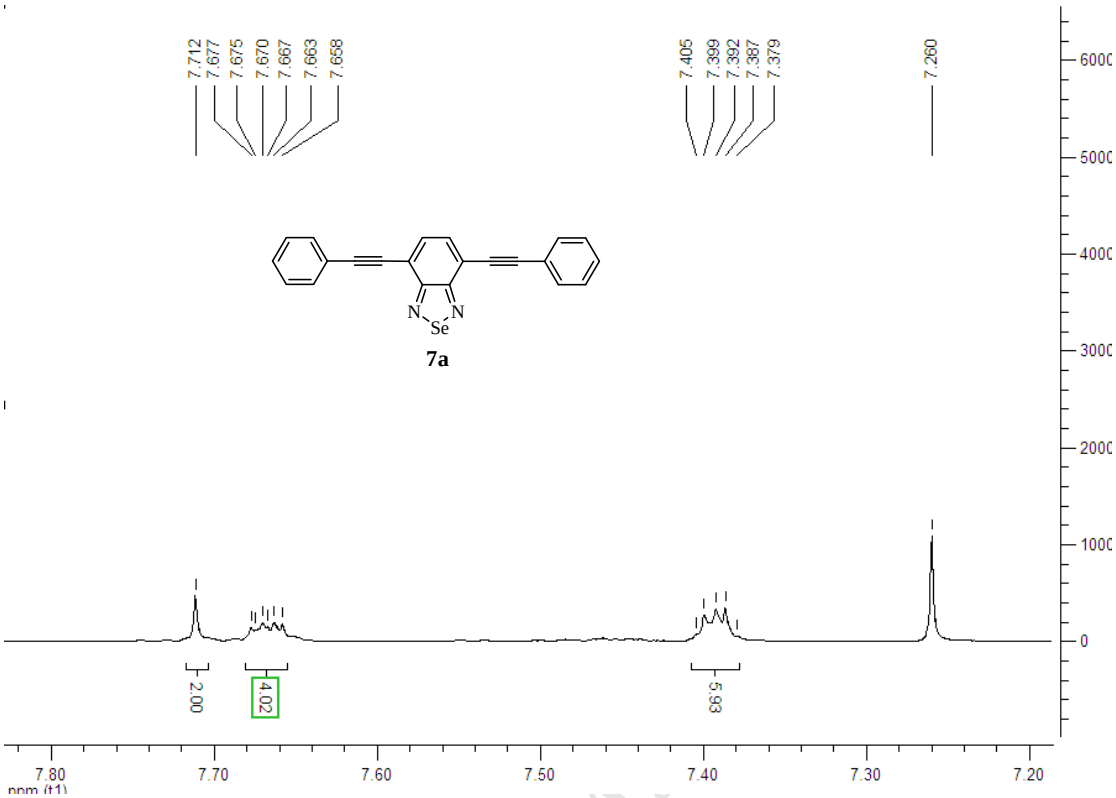

Fig. S6. ^{1}H NMR of **7a** ($CDCl_3$, 500 MHz)

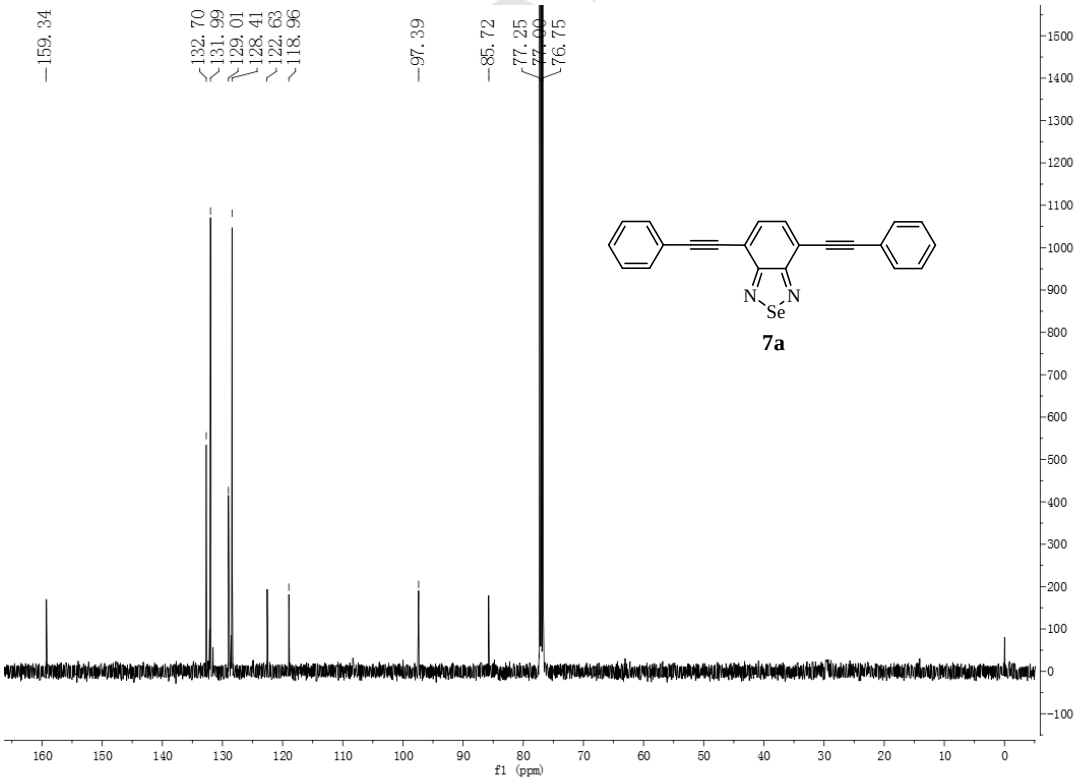

Fig. S7. ^{13}C NMR of **7a** ($CDCl_3$, 125 MHz)

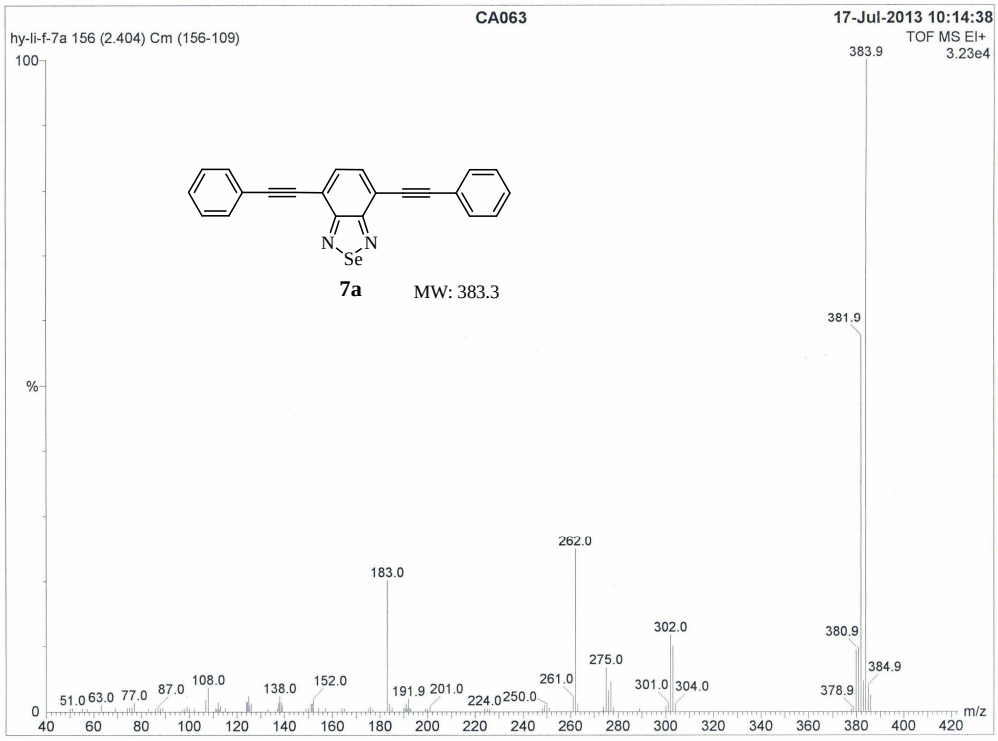

Fig. S8. MS spectra of **7a**

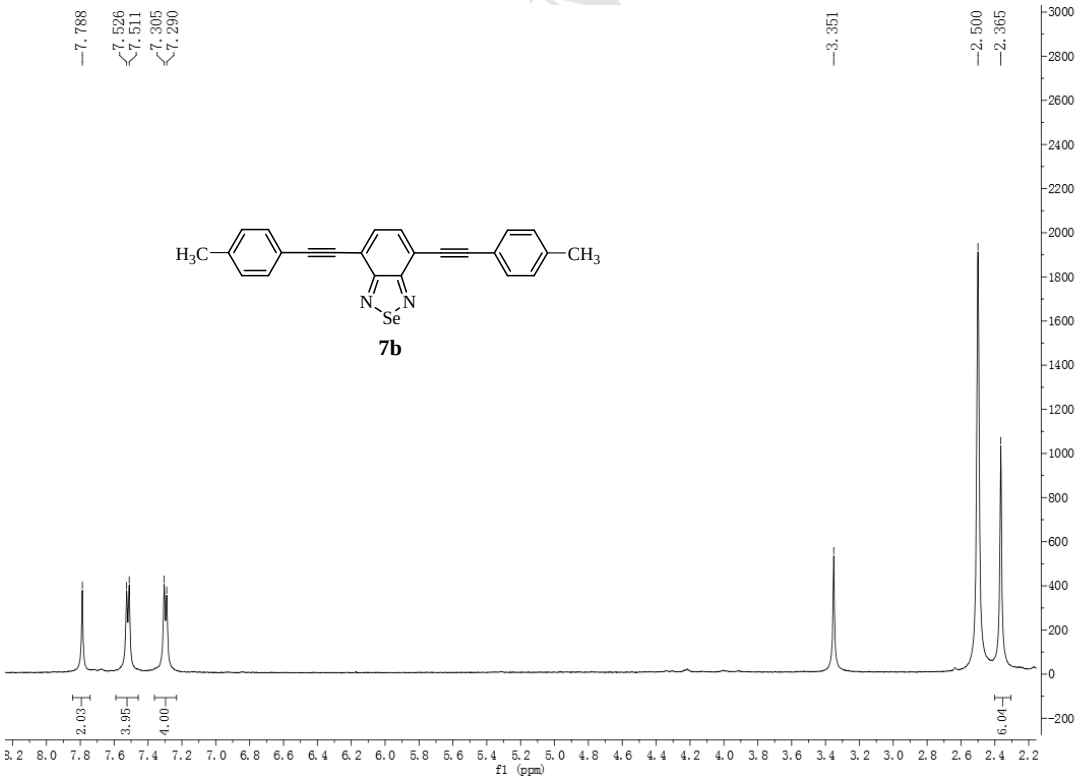

Fig. S9. ^{1}H NMR of **7b** (DMSO-d_6, 500 MHz)

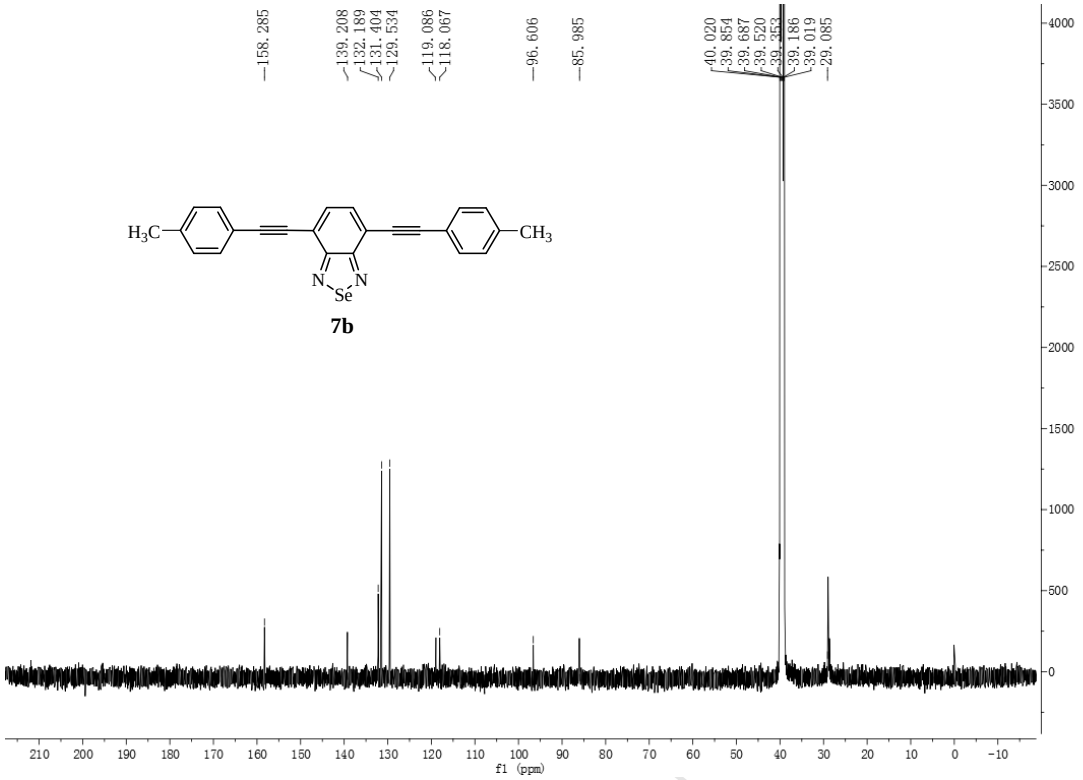

Fig. S10. ^{13}C NMR of **7b** (DMSO-d_6, 125 MHz)

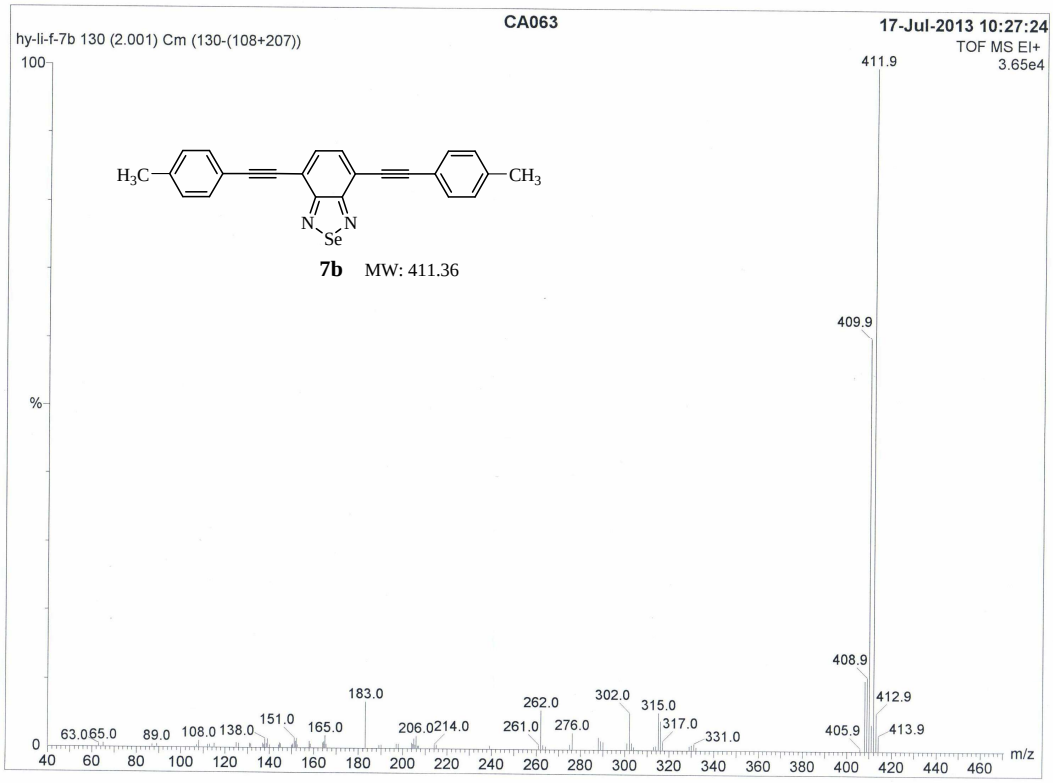

Fig. S11. MS spectra of **7b**

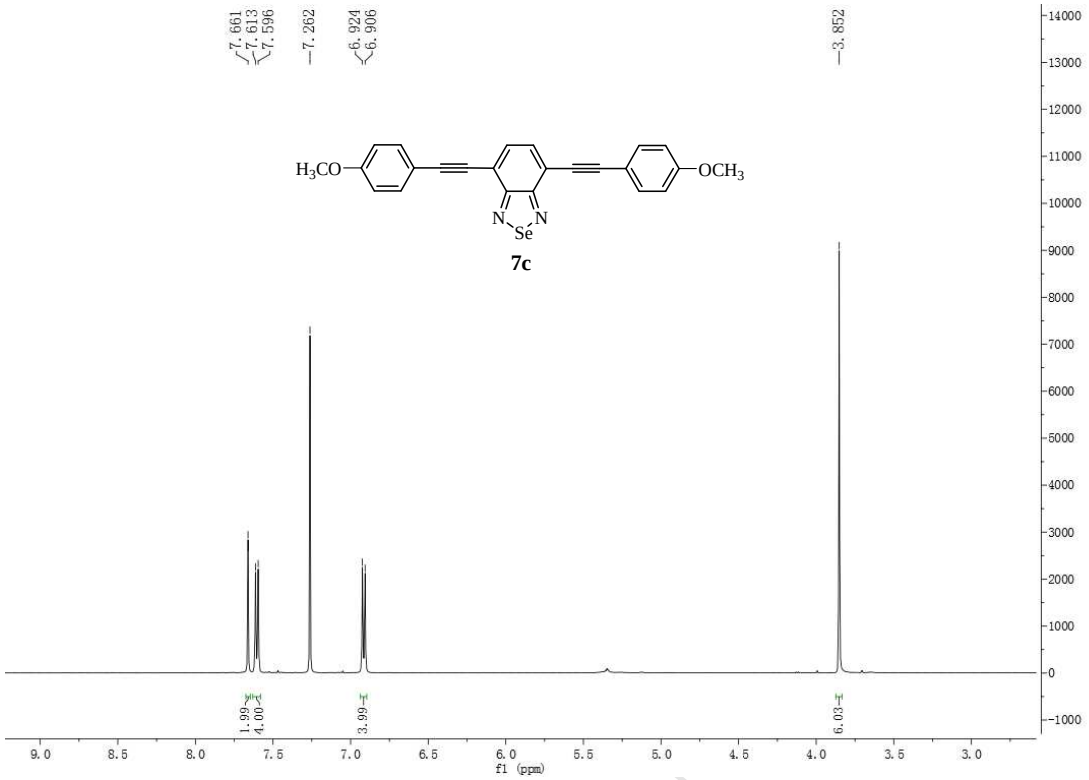

Fig. S12. ^{1}H NMR of **7c** ($CDCl_3$, 500 MHz)

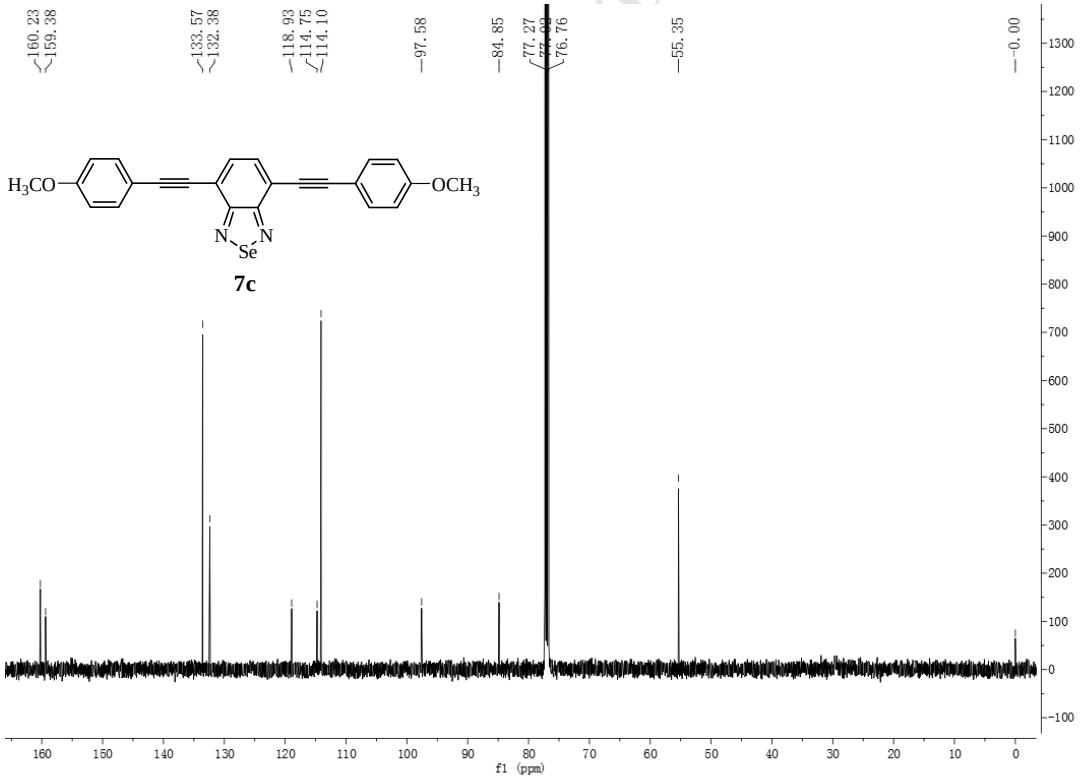

Fig. S13. ^{13}C NMR of **7c** ($CDCl_3$, 125 MHz)

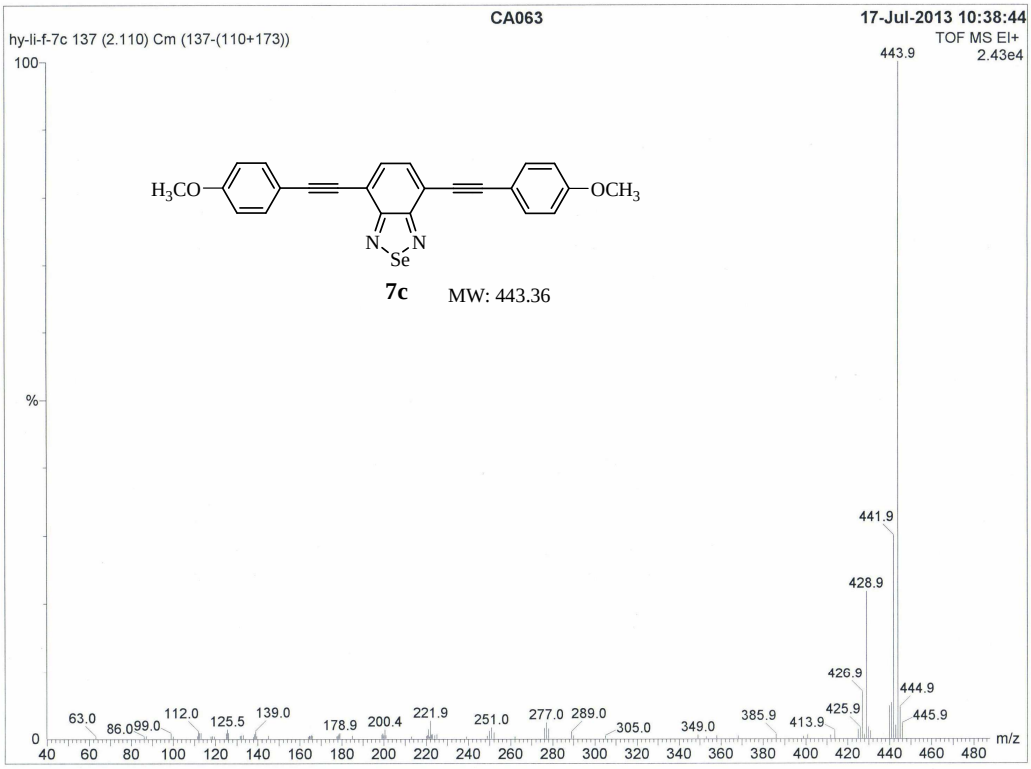

Fig. S14. MS spectra of **7c**

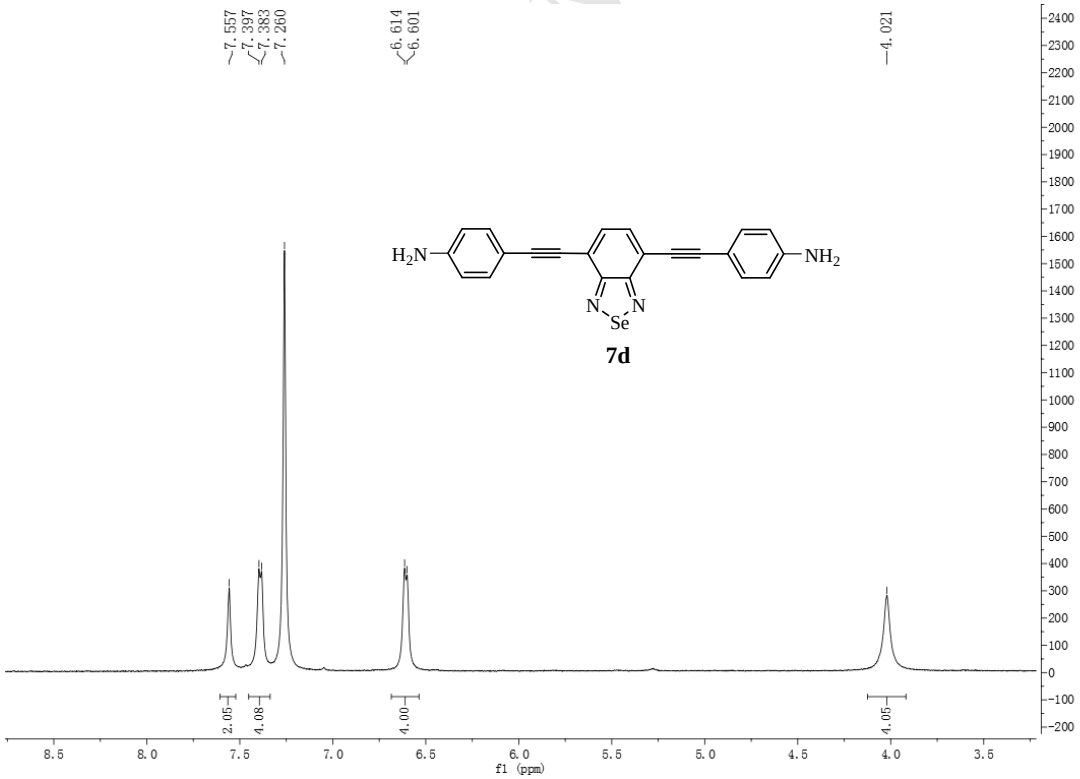

Fig. S15. ^{1}H NMR of **7d** ($CDCl_3$, 500 MHz)

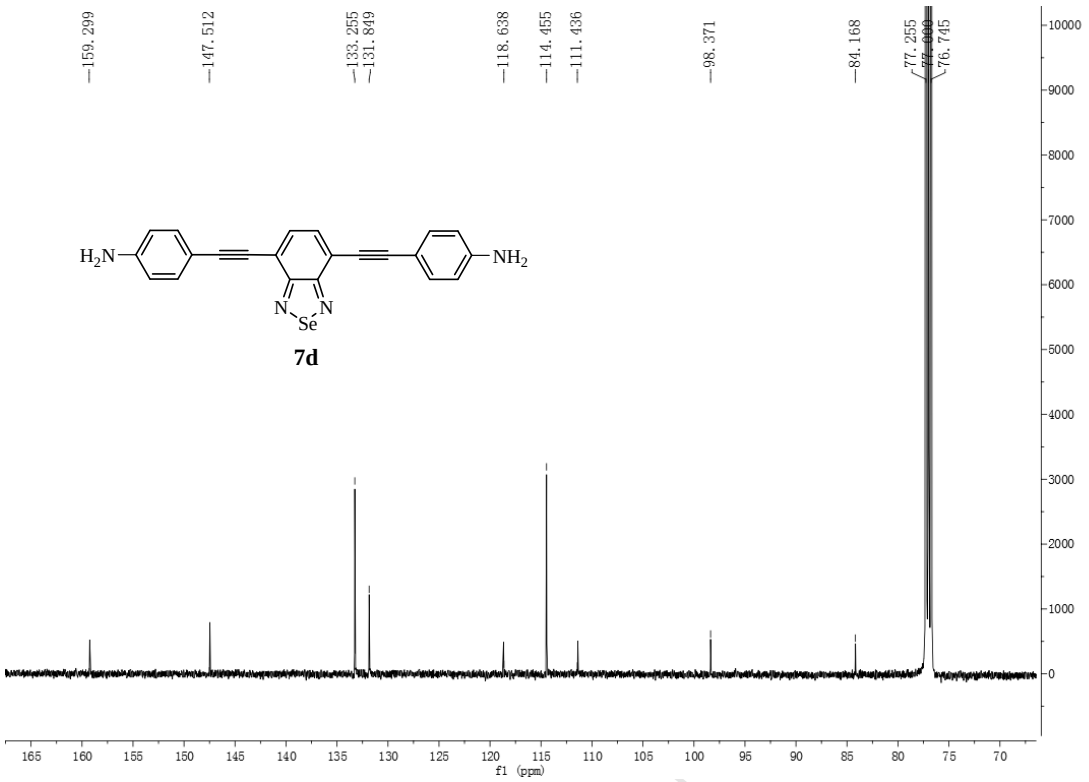

Fig. S16. ^{13}C NMR of **7d** ($CDCl_3$, 125 MHz)

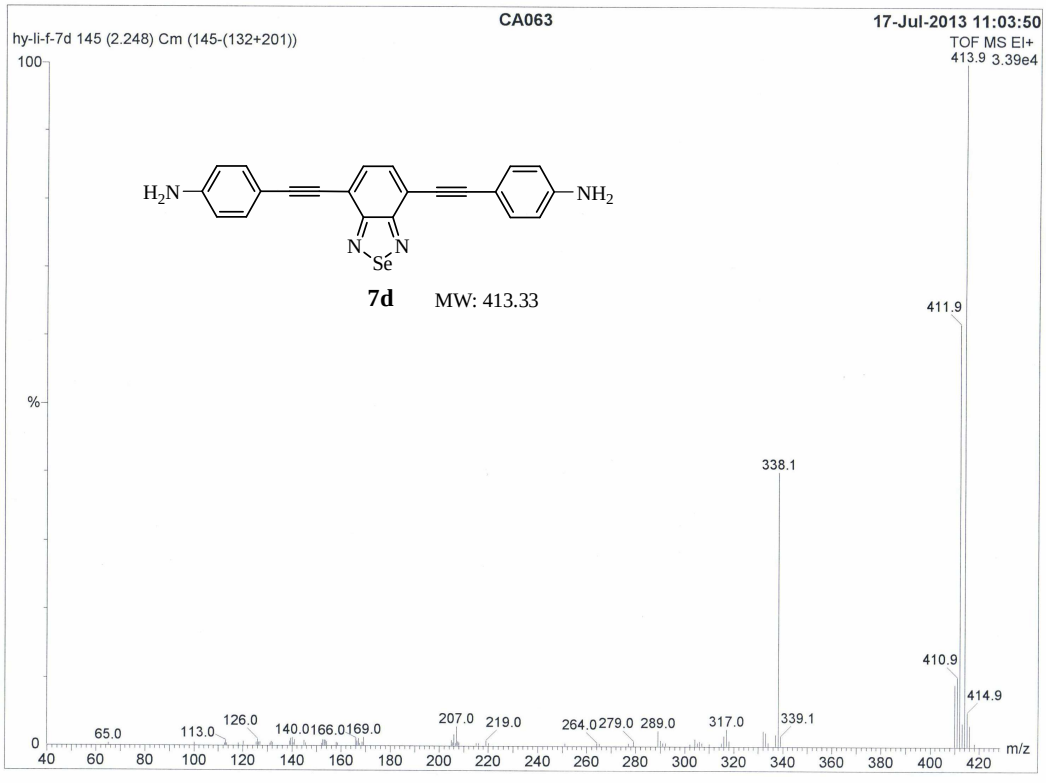

Fig. S17. MS spectra of **7d**

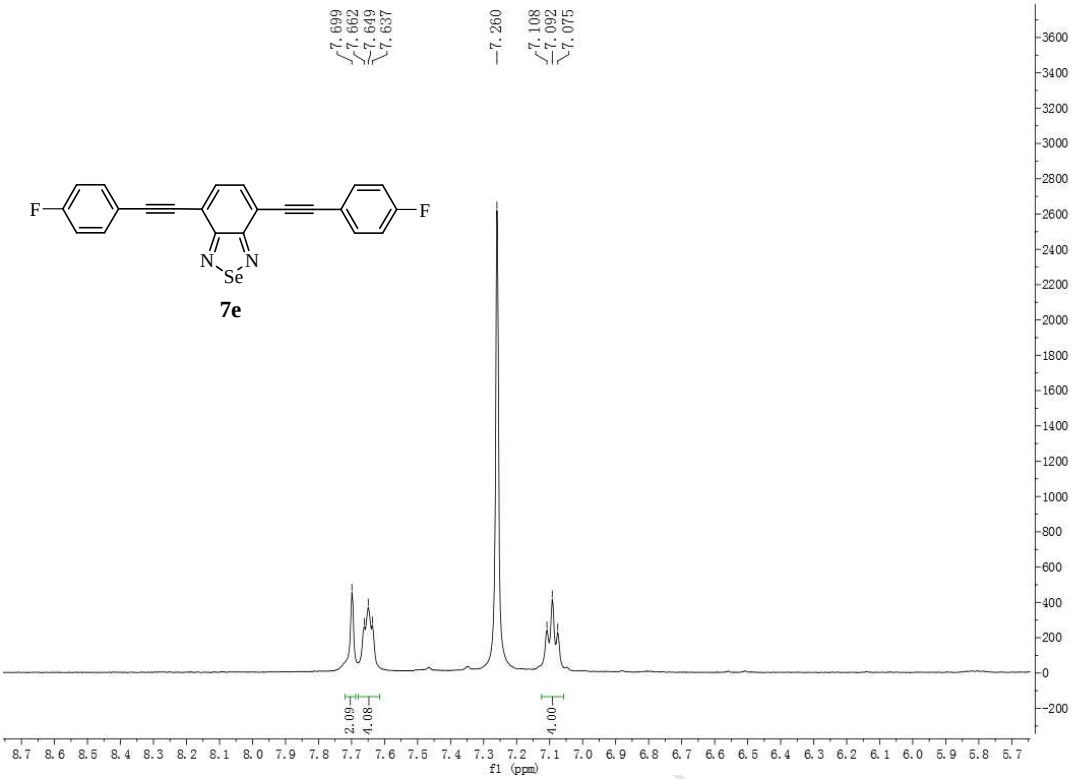

Fig. S18. ^{1}H NMR of **7e** ($CDCl_3$, 500 MHz)

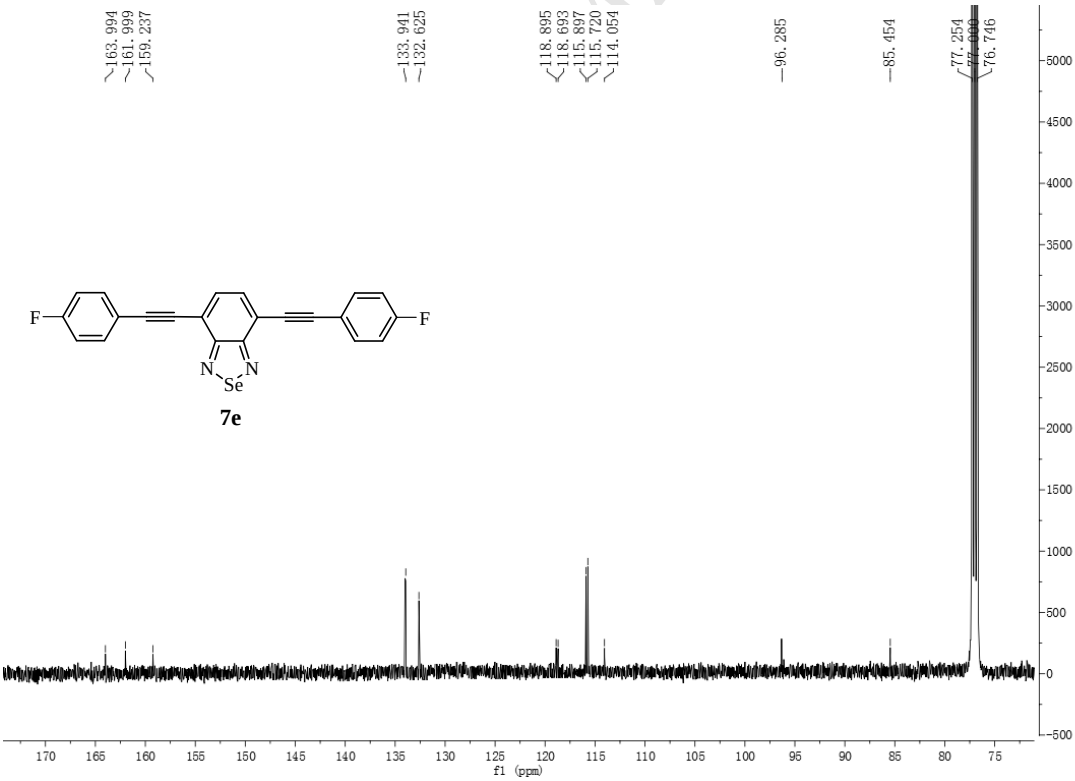

Fig. S19. ^{13}C NMR of **7e** ($CDCl_3$, 125 MHz)

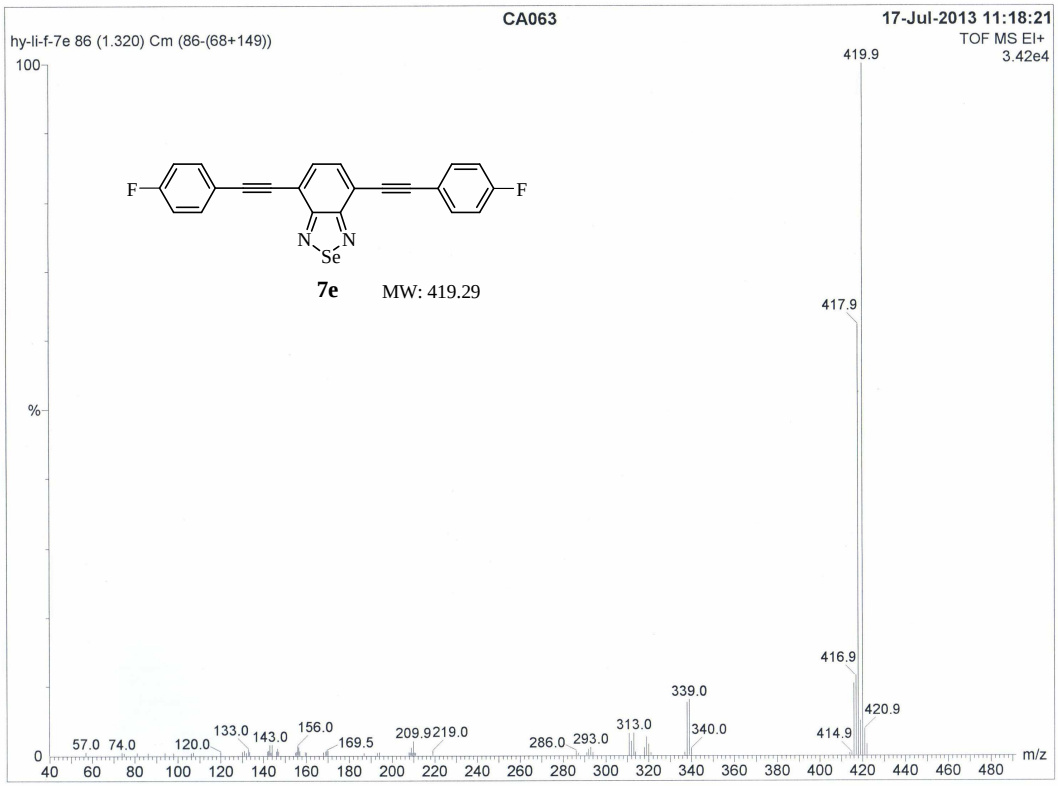

Fig. S20. MS spectra of **7e**

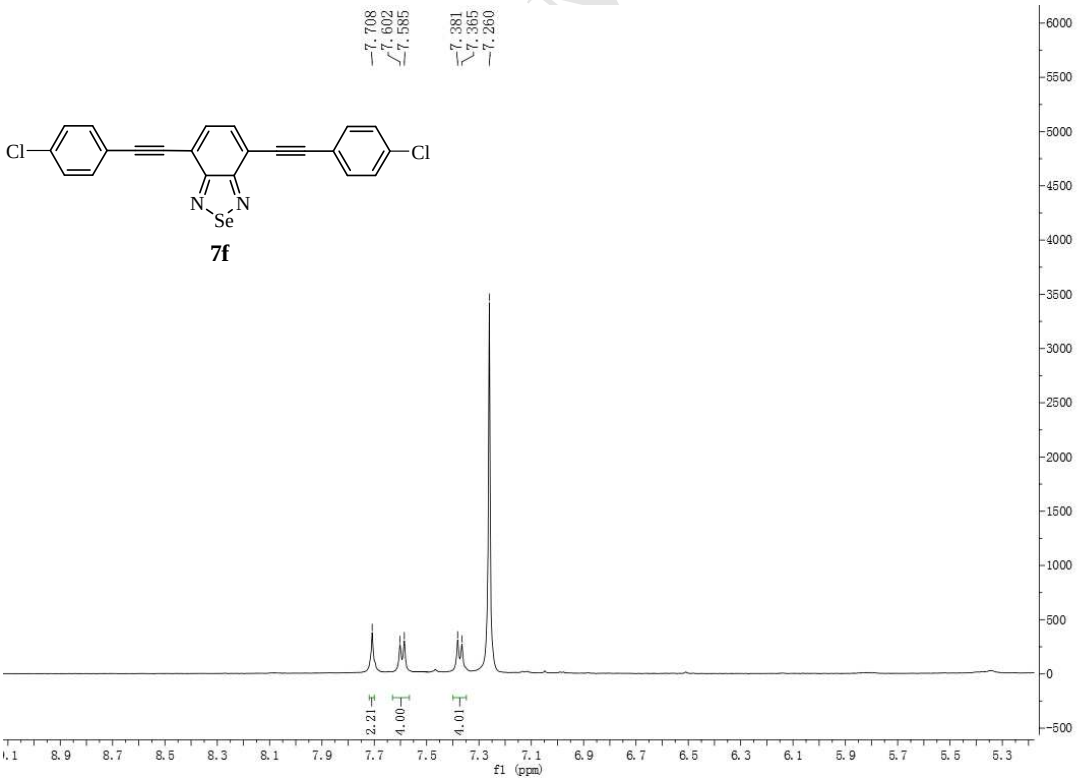

Fig. S21. ^{1}H NMR of **7f** ($CDCl_3$, 500 MHz)

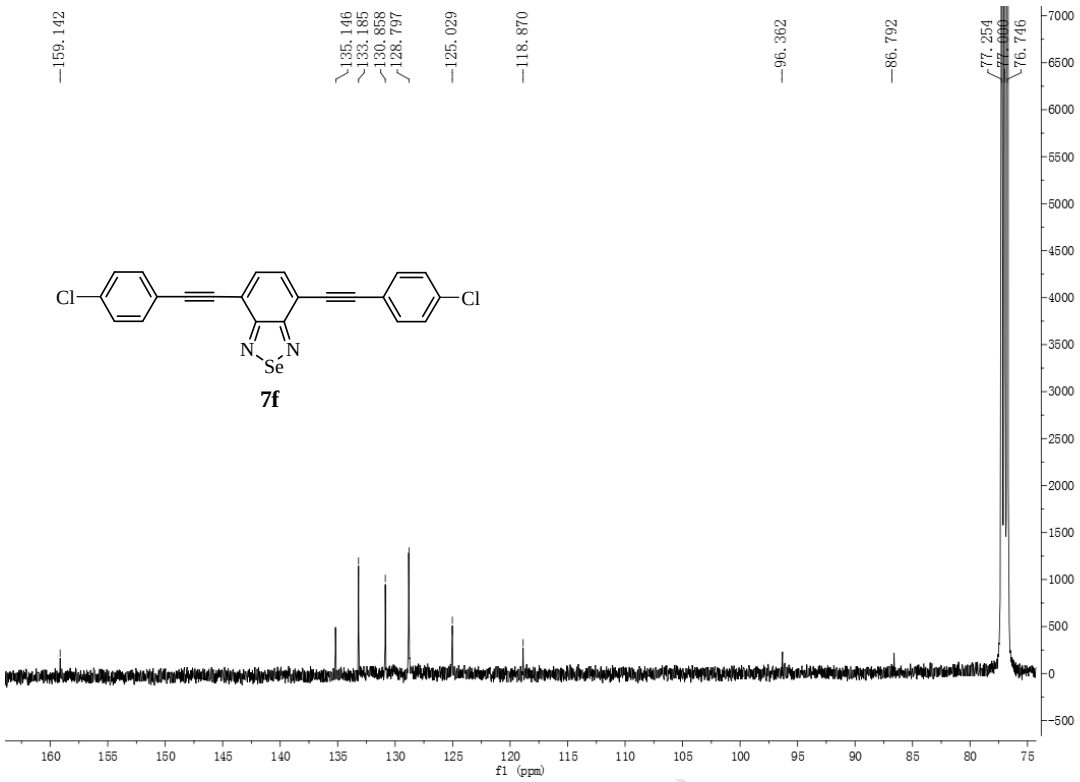

Fig. S22. ^{13}C NMR of **7f** ($CDCl_3$, 125 MHz)

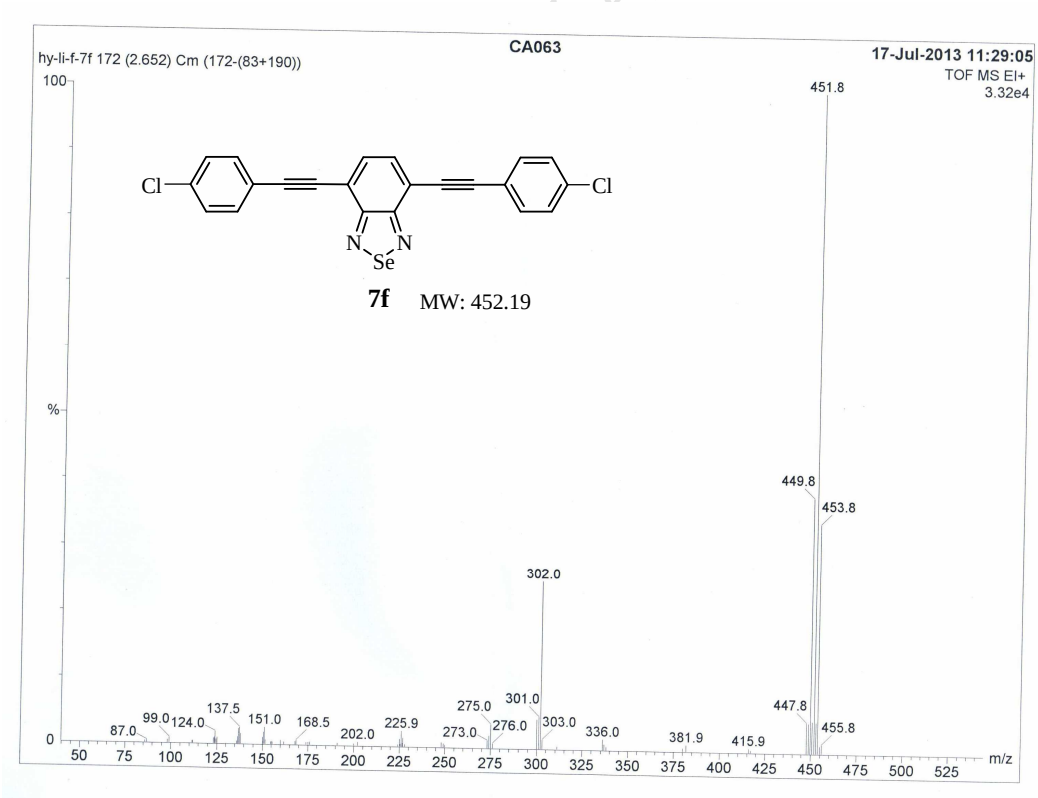

Fig. S23. MS spectra of **7f**

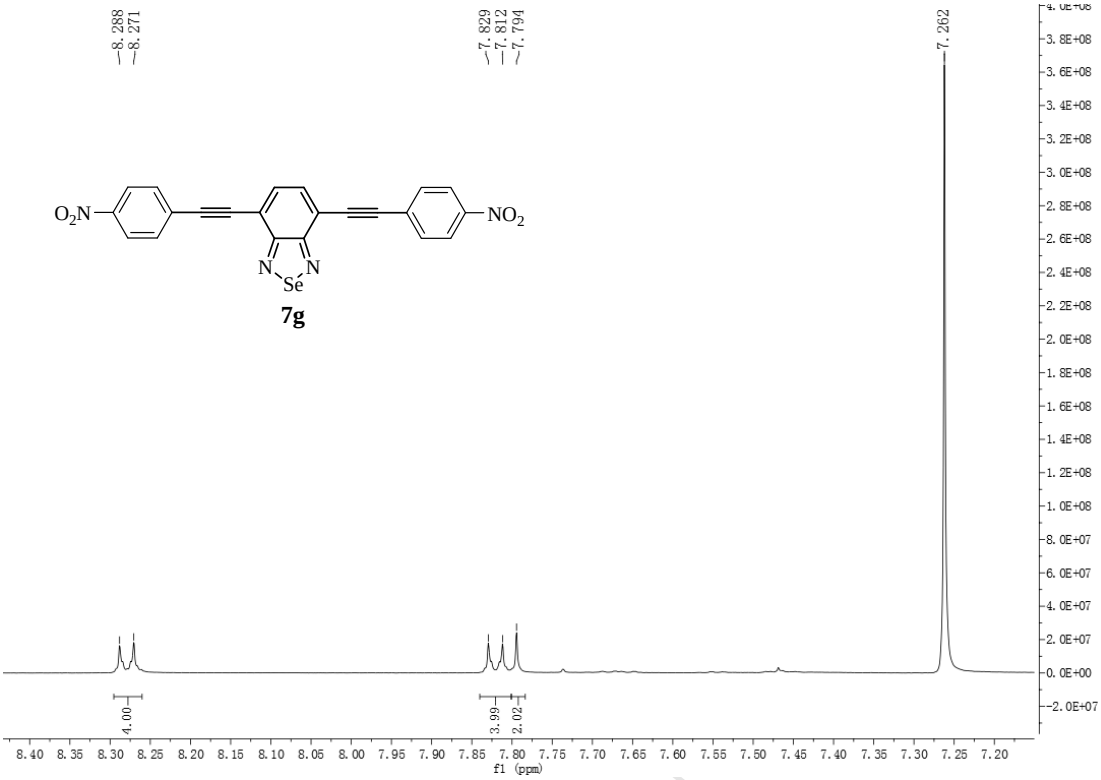

Fig. S24. ^{1}H NMR of **7g** ($CDCl_3$, 500 MHz)

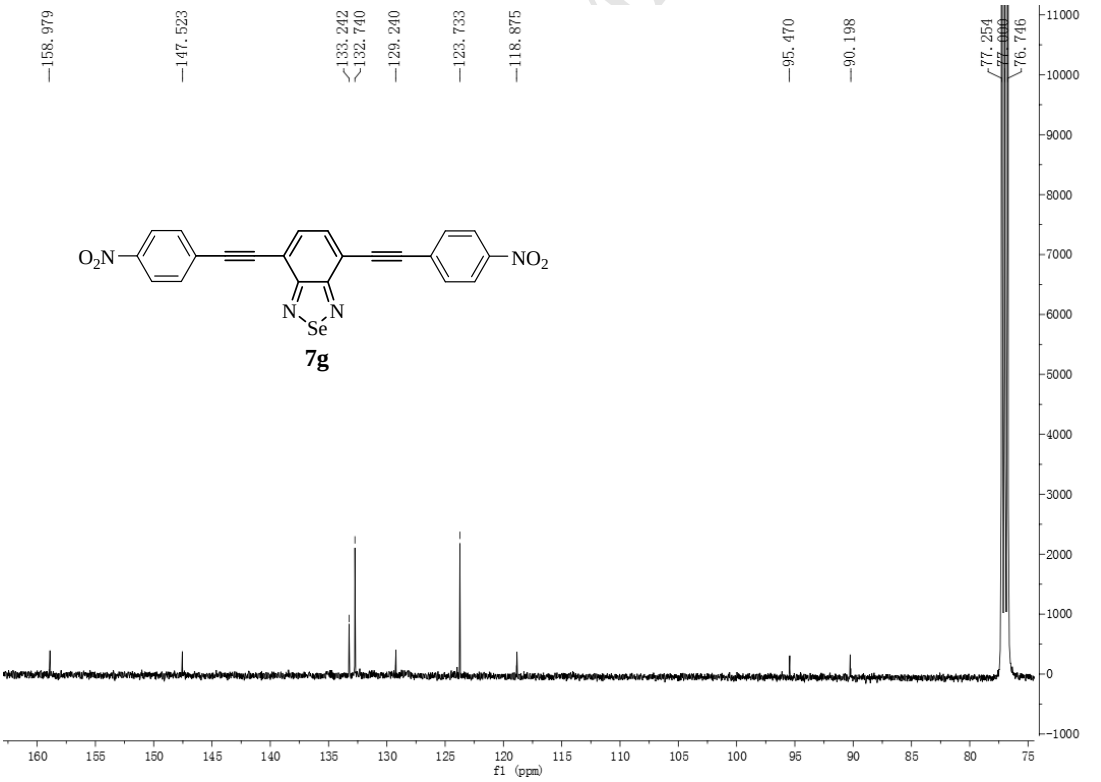

Fig. S25. ^{13}C NMR of **7g** ($CDCl_3$, 125 MHz)

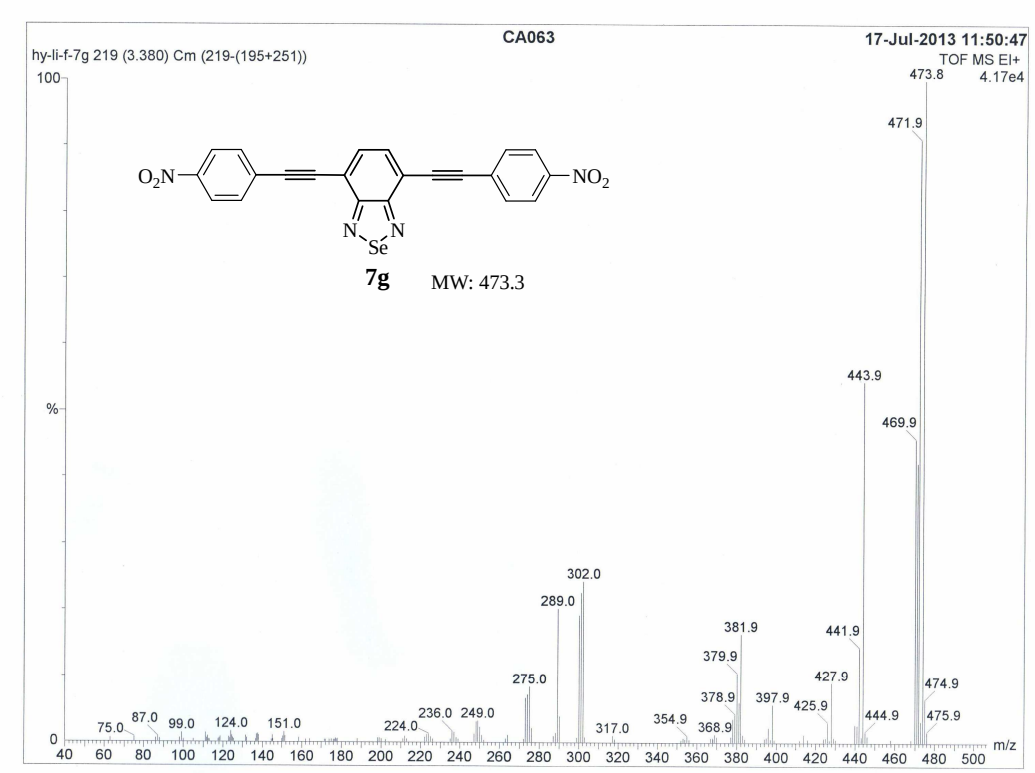

Fig. S26. MS spectra of **7g**

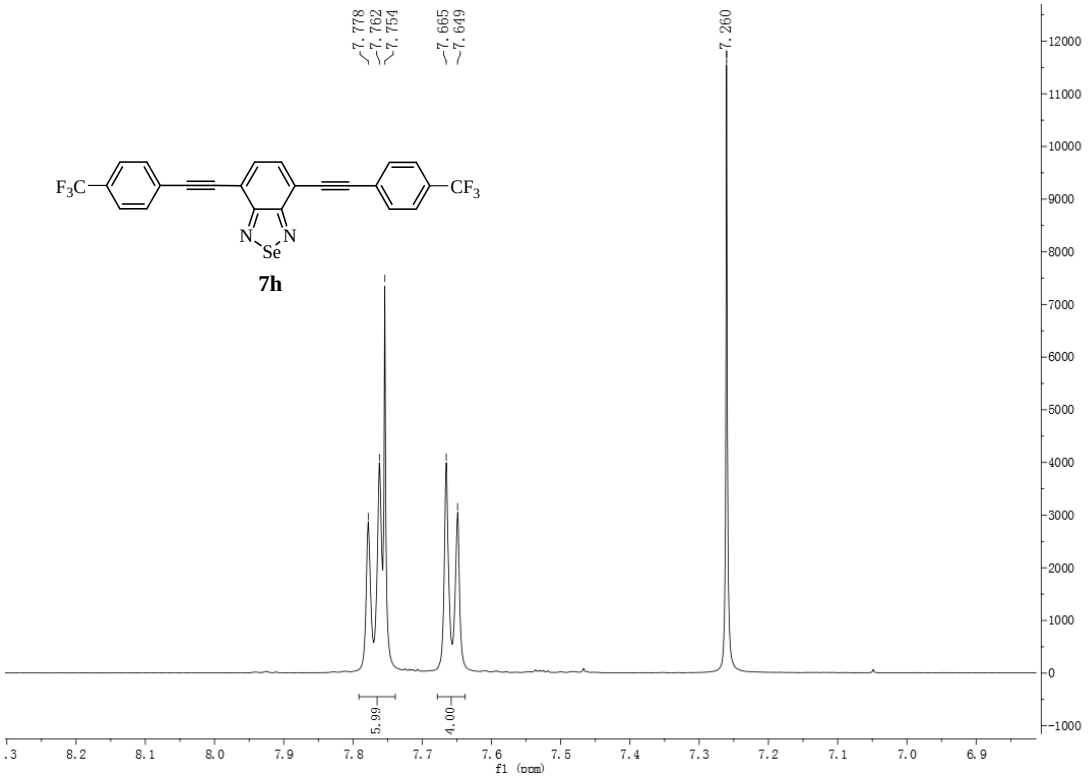

Fig. S27. ^{1}H NMR of **7h** ($CDCl_3$, 500 MHz)

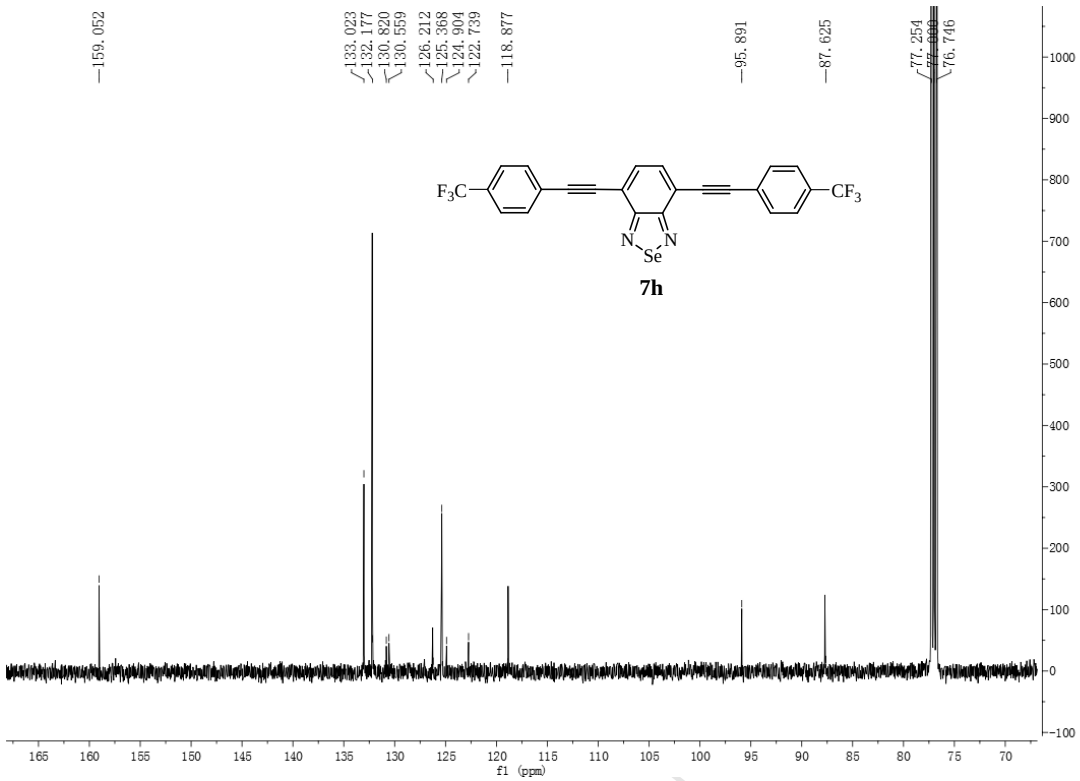

Fig. S28. ^{13}C NMR of **7h** ($CDCl_3$, 125 MHz)

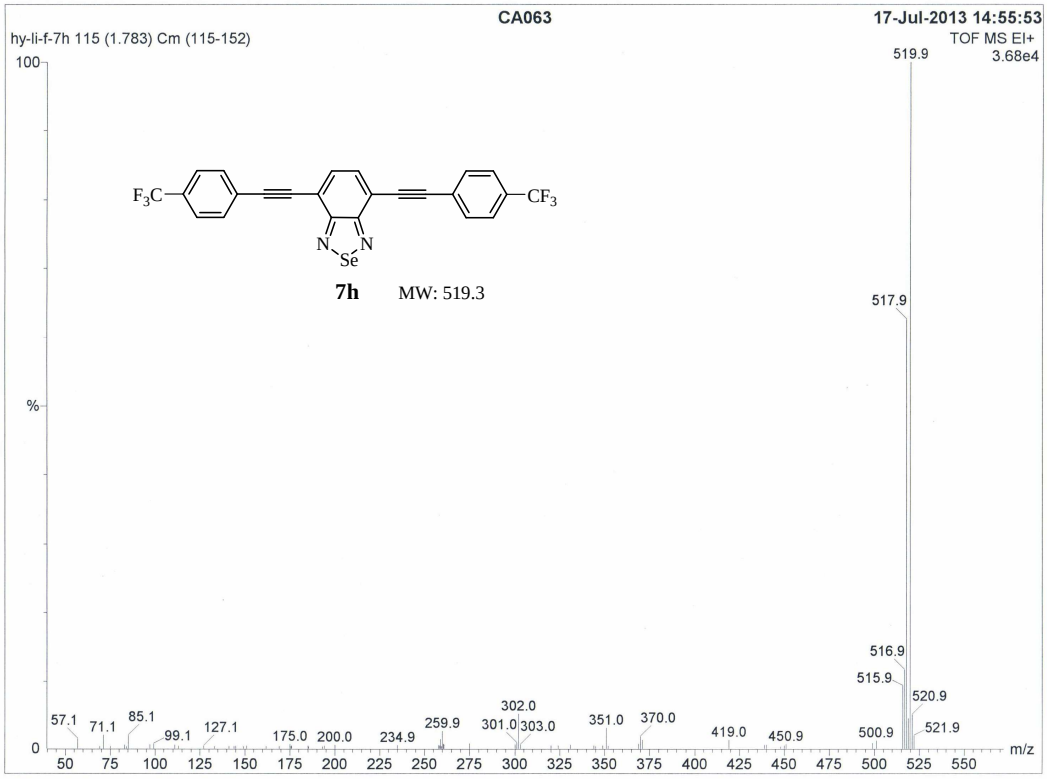

Fig. S29. MS spectra of **7h**

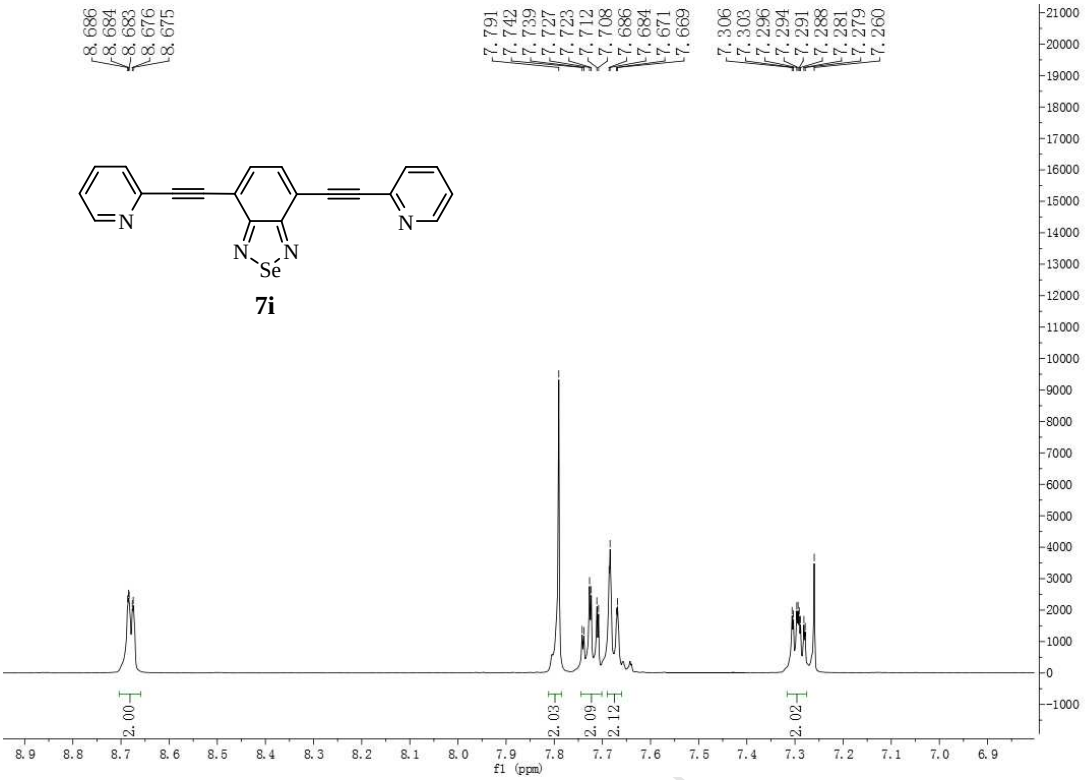

Fig. S30. ^{1}H NMR of **7i** ($CDCl_3$, 500 MHz)

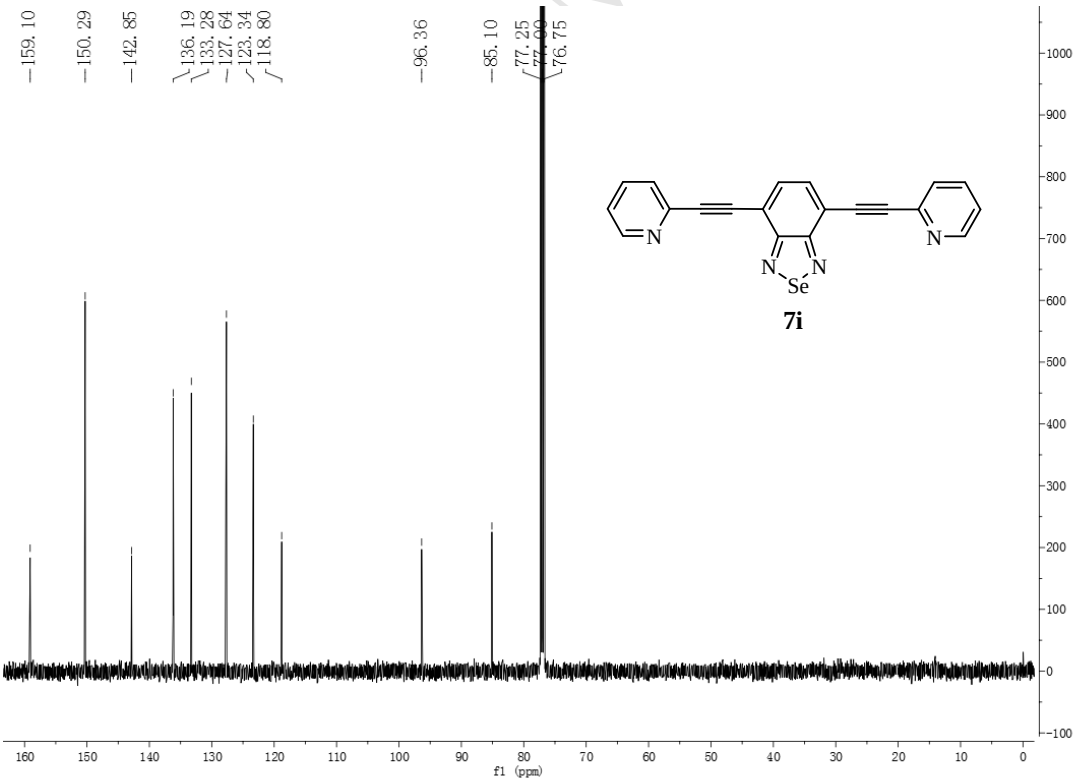

Fig. S31. ^{13}C NMR of **7i** ($CDCl_3$, 125 MHz)

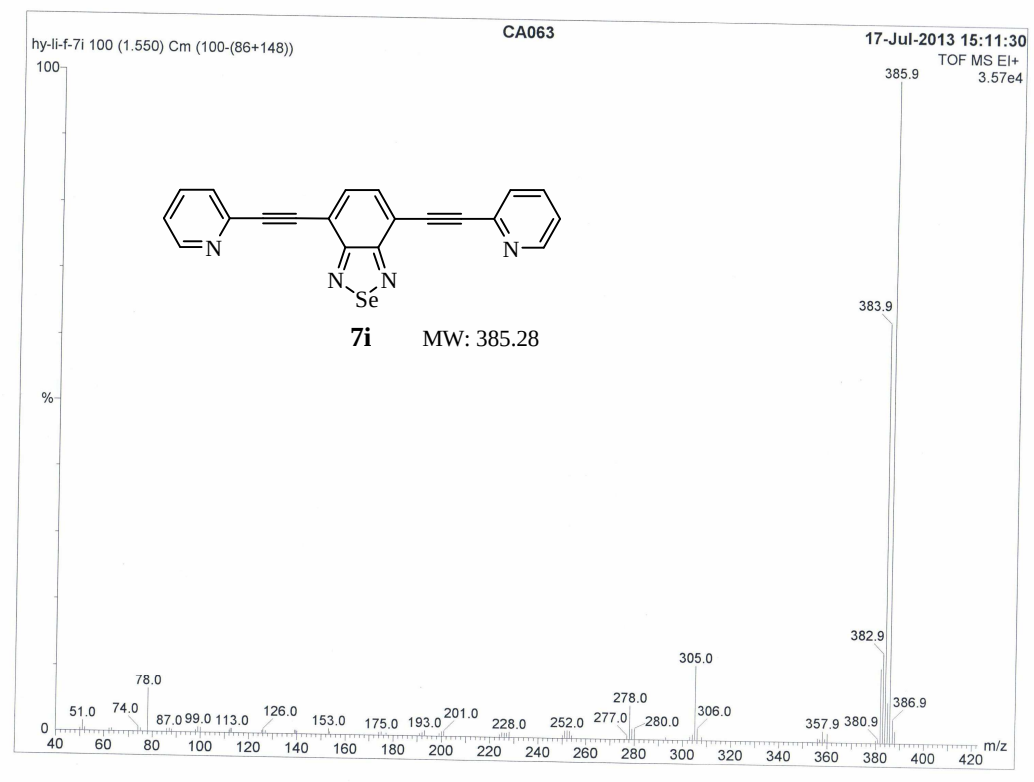

7i MW: 385.28

Fig. S32. MS spectra of **7i**